Single cell RNA-sequencing of feline peripheral immune cells with V(D)J repertoire and cross species analysis of T lymphocytes

Raneesh Ramarapu[1,2], Judit M. Wulcan[3], Haiyang Chang[4], Peter F. Moore[3], William Vernau[3], Stefan M. Keller[3]

[1]Department of Surgical and Radiological Sciences, School of Veterinary Medicine, University of California Davis, Davis, CA, USA.

[2]Department of Anatomy, Physiology and Cell Biology, School of Veterinary Medicine, University of California Davis, Davis, CA, USA.

[3]Department of Pathology, Microbiology and Immunology, School of Veterinary Medicine, University of California, Davis, CA, United States.

[4]Department of Mathematics and Statistics, University of Guelph, Guelph, ON, Canada.

1 Abstract

Introduction. The domestic cat (Felis catus) is a valued companion animal and a model for virally induced cancers and immunodeficiencies. However, species-specific limitations such as a scarcity of immune cell markers constrain our ability to resolve immune cell subsets at sufficient detail. The goal of this study was to characterize circulating feline T cells and other leukocytes based on their transcriptomic landscape and T-cell receptor repertoire using single cell RNA-sequencing.

Methods. Peripheral blood from 4 healthy cats was enriched for T cells by flow cytometry cell sorting using a mouse anti-feline CD5 monoclonal antibody. Libraries for whole transcriptome, alpha/beta T cell receptor transcripts and gamma/delta T cell receptor transcripts were constructed using the 10x Genomics Chromium Next GEM Single Cell 5' reagent kit and the Chromium Single Cell V(D)J Enrichment Kit with custom reverse primers for the feline orthologs.

Results. Unsupervised clustering of whole transcriptome data revealed 7 major cell populations - T cells, neutrophils, monocytic cells, B cells, plasmacytoid dendritic cells, mast cells and platelets. Sub cluster analysis of T cells resolved naive (CD4+ and CD8+), CD4+ effector T cells, CD8+ cytotoxic T cells and gamma/delta T cells. Cross species analysis revealed a high conservation of T cell subsets along an effector gradient with equitable representation of veterinary species (horse, dog, pig) and humans with the cat. Our V(D)J repertoire analysis demonstrated a skewed T-cell receptor alpha gene usage and a restricted T-cell receptor gamma junctional length in CD8+ cytotoxic T cells compared to other alpha/beta T cell subsets. Among myeloid cells, we resolved three clusters of classical monocytes with polarization into pro- and anti-inflammatory phenotypes

in addition to a cluster of conventional dendritic cells. Lastly, our neutrophil sub clustering revealed a larger mature neutrophil cluster and a smaller exhausted/activated cluster.

Discussion. Our study is the first to characterize subsets of circulating T cells utilizing an integrative approach of single cell RNA-sequencing, V(D)J repertoire analysis and cross species analysis. In addition, we characterize the transcriptome of several myeloid cell subsets and demonstrate immune cell relatedness across different species.

Keywords: feline, T cells, single cell RNA-sequencing (scRNA-seq), T-cell receptor repertoire, cross species analysis, myeloid cells, V(D)J

2 Introduction

The domestic cat, Felis catus, is a valued companion animal and the second most popular pet in the United States. As of the American Veterinary Medicine Association (AVMA) pet ownership statistics, there are upwards of 46.5 million households with at least one cat in 2023 with ownership trends rising in the last decade from 25% in 2016 to 29% in 2022 (1,2). In addition to the growing need for feline veterinary care, the cat is an important model for infectious diseases such as virally-induced cancers (Feline leukemia virus, FeLV) and virally mediated immunodeficiency (Feline immunodeficiency virus, FIV) (3–6). Despite the value of the cat as a companion animal and infectious disease model, there are species specific research limitations including few cat-reactive immunophenotyping reagents and a poor knowledge base of immune cell markers and behavior.

In the advent of deciphering the feline immune system, many studies characterizing feline immune cells have relied strongly on antibody-based assays including flow cytometry and immunohistochemistry. This has allowed the study of immune cells in health and disease conditions such as FeLV or FIV (7–9). This approach depends on the assumption that feline immune cells are similar to other species. However, feline immune mediated diseases behave very differently from those in other small animals such as dogs, exhibiting unique etiologies and pathogenesis (10). In a cross-species context, innate immunity shows relatively high evolutionary conservation; however, this conservation dwindles with progression to adaptive immunity and complex immune phenotypes (11). Additionally, there is growing evidence demonstrating that evolutionary relationships do not translate to immune transcriptional or cell type relationships. Such an example is the mouse being a better model for human immune cells than the macaque (12). Thus, understanding the species-specific system in the context of our growing evolutionary database is desirable and there is a strong need to characterize the heterogeneous peripheral immune cell population in the cat, especially diverse populations such as T cells.

In efforts to investigate feline specific T cell diseases, our laboratory has contributed to the growing feline specific reagent and immune cell knowledge base including T cell receptor (TCR) repertoire analysis (13). In this trajectory, single cell RNA-sequencing is a logical next step. It enables the efficient large-scale capture and analysis of heterogeneous tissues, overcoming the challenges of species-specific reagent assays (14–17). Consequently, there has been a bloom in single cell RNA-sequencing studies of the peripheral leukocytes in a variety of mammalian species including the dog, cow, horse, and pig (18–22). Additionally, single cell data facilitates the study of cross species variations in immune cell type and evolution of these cells (12). ScRNA-seq of feline circulating leukocytes have been previously performed demonstrating the presence of 5 major cell types (T cells, B cells, NK cells, monocytes, dendritic cells) in the context of other non-model species (23). However, in-depth characterization of key subtypes and their marker conservation is yet to be determined. Thus, the goal of this study is to characterize the heterogeneity of circulating feline T cells and other captured leukocytes utilizing CD5 flow cytometry enriched scRNA-seq and V(D)J repertoire analysis in clinically healthy domestic shorthair cats between the ages of 6 months and 9 years. CD5 was chosen as a selective T-cell marker given the lack of availability of anti-feline CD3 antibodies. Additionally, we performed a cross species transcriptomic integration to assess feline T cells in the context of 4 other mammalian species - dog, horse, human, and pig. Our results provide a foundation for feline immune transcriptomics.

3 Results

3.1 Single cell atlas of the feline circulating immune cells

ScRNA-seq data obtained from 4 representative healthy cats of different ages consisted of 30,073 quality cells. These age groups were selected as they capture the major feline life stages: 6-month-old juvenile (6MO), 1-year-old mature (1YO), 4-year-old adult (4YO), and 9-year-old aged (9YO). The average number of cells captured per cat was 7,518 with an average of 3,655 transcripts per cell. **<Fig1A, Supplementary File1 S1A,B>**. Due to the poor annotation of the cat reference genome, we utilized a custom homologous mapping script based on ENSEMBL homologous mapping between the cat and human to improve gene readability. Our script increased the number of gene symbols mapped from 13,886 to 16,936, improving the quality of cell type assignment and biological interpretation. Following batch correction via reciprocal principal component analysis, unsupervised clustering revealed the presence of 21 clusters **<Fig 1B>**. A majority of cell types are equally represented from each sample **<Fig1C, 1D>**. A quality control violin plot for clusters can be found in the supplementary materials **<Supplementary File1 S2A>**.

These clusters were categorized into 7 major immune cell types based on canonical marker genes from multi-species PBMC single cell literature, top marker genes and over-enrichment gene ontology (GO) **<Supplementary File 2,3>**. The most numerous cell type identified was T cells called by high expression of T cell receptor complex genes (*CD3D, CD3E*) and species conserved T cell markers *LCK*, *ITK* and *TCF7* (12,23) **<Fig 1E-G, Supplementary File1 S2B>**. Across most T cell clusters, top identified GO terms of biological processes (BP) included T leukocyte

processes of differentiation, migration, activation, and effector functions **<Supplementary File 3>**.

The second most abundant population was the neutrophils marked by neutrophil-derived proteases including elastase (*ELANE*), granulocyte colony stimulating factor receptor (*CSF3R*) and calprotectin (*S100A8/S100A9*) (24–26) **<Fig 1E,H>**. In most species, neutrophils are not captured in the PBMC layer during density centrifugation (27). Interestingly, our single cell data set captured a significant number of neutrophils from all but the 1YO sample **<Fig 1D>**. This is the first description of feline neutrophils at the single cell transcriptomic level and can provide insights into biological processes of these abundant cells.

A substantial number of monocytic cells were captured with marker genes including scavenger receptor for haptoglobin-hemoglobin complexes *CD163*, antigen presenting cell co-stimulatory molecule *CD83*, lipopolysaccharide detector protein *CD14*, phospholipase B domain containing 1 (*PLBD1*) and colony stimulating factor receptor (*CSF1R*) (28,29) **<Fig 1E,I,J>**. A relatively small but heterogeneous population of B cells were captured which were identified by conserved markers including B cell surface molecule *MS4A1* and Ig-alpha protein of the B-cell antigen component *CD79A* (23) **<Fig 1E,K,L>**. This population also expresses immunoglobulin genes (*IGHG3, IGHM*) indicating a sub-population of plasma cells (12) **<Fig 1E>**.

Unexpectedly, we captured plasmacytoid dendritic cells (pDC) and mast cells, which represented rare but discrete cell populations. pDCs were identified by expression of Fc fragment of gamma immunoglobulin (*FCRLA)*, dendritic marker *PLAC8B*, and immunoglobulin lambda constant 7 (*IGLC7*) and lack of expression of B cell canonical markers *MS4A1* and *CD79A* (30–32) **<Fig 1E,L,M>**. pDcs clustered more closely with B cells than other myeloid cells. This is due to close lineage associations and the shared expression of integral markers *FCRLA* and *IGLC7* among others (33) **<Fig 1E,L>**. Currently, there is debate regarding the reclassification of pDCs as innate lymphocytes and this analysis further supports such an argument (34) **<Fig1B>**. Mast cells were marked by IgE receptor *MS4A2* and a key component of mast cell protease, *CPA3* (35,36) **<Fig 1E,N>**.

Lastly, we captured a population of non-leukocytic immune cells which were annotated as platelets due to high expression of platelet specific proteins *PPBP*, *VWF* and *GP9* (37) **<Fig1E,O>**. This cluster also exhibited an extremely low average count of unique RNA and total RNA, which is consistent with a highly specialized cell type lacking a nucleus **<Supplementary File1 S2A>**.

3.2 Feline circulating T cells

To further characterize T cell subsets, we independently analyzed T cell clusters previously described at the global level (clusters 0,2,9,1,6,4,5,14,8,12, and 15). Unsupervised clustering of T cells revealed the presence of seven T cell clusters, which were unrecognizable at the global level

<Fig 2A>. Largely, these clusters represent greater T cell phenotypes along increasing pseudotime values (proxy of differentiation or lineage) **<Fig 2B,C>**. The subtle transcriptional differences, as noted through overlapping differentially expressed genes, make effective annotation difficult **<Supplementary File 4>**. Nonetheless, we were able to identify several canonical subsets.

T cell subsets included *CD4*$^+$, *CD8A*$^+$/*CD8B*$^+$ and γδ T cells and were equally represented in all age groups **<Fig2D-H>**. A great majority were identified as naive cells, distinguished by their high expression of *CCR7* and L-selectin (*SELL*) (38–40) **<Fig2I,J>**. These naive populations segregated into two larger groups which could be distinguished by differential expression of *CD4* and *CD8A*/*CD8B* **<Fig2F-H>**. The *CD8A*$^+$/*CD8B*$^+$ naive population represents a divergence from the traditionally observed distribution of naive T cells. Most naive T cells in mammalian species are *CD4*$^+$ (12). However, a large population of *CD8A*$^+$/*CD8B*$^+$ naive cells has been described in non-model species such as the horse (22). This highlights a potentially influential role of *CD8A*$^+$/*CD8B*$^+$ T cells in cats.

The clusters 3 and 4, adjacent to the large naive populations, were identified as effector cells (T_{EM}) **<Fig2A>**. These clusters show a gradual upregulation of T effector molecules including *S100A11,* galectins (*LGALS1, LGALS3),* annexins (*ANXA1, ANXA2*), and granzymes (*GZMA, GZMK*) (41,42) **<Fig2C,K-M>**. Szabo et al identified *CCL5* as a critical marker for highly differentiated effector T cells across tissues as well as its antagonistic expression to the naive marker *SELL* (41). In our data, Cluster 6 expressed the highest levels of cytotoxic markers including *CCL5* and exhibited the highest pseudotime score with no naive marker expression **<Fig2C,M-O>**. This indicates that this cluster is most consistent with the annotation of a terminally differentiated T cell cluster (CD8$^+$ cytotoxic). Additionally, some effector cells expressed genes associated with T cell exhaustion such as *PDCD1* and *TIGIT* indicating the presence of a few of these cells in circulation **<Fig2C,P,Q>**.

Cluster 5 represented γδ T cells as inferred by the overlapping expression of the TCR genes *TRG* and *TRDC* (13) **<Fig2E>**. Within this population, there was an expression gradient of naive as well as effector markers, indicating subtypes within the γδ population **<Fig 2I,K,L>**. Although these T cell clusters represent biologically relevant groups statistically, the literature across various species identifies significant challenges associated with clustering of transcriptionally similar but heterogenous T cell populations (43). The γδ cluster exemplifies this challenge in that the cluster's defining features overlap between two different but not mutually exclusive phenotypes - γδ recombination and effectorness/naiveness. These cells exhibit overlapping expressions of *TRG* and *TRDC*, indicating their TCR recombination-based categorization. An overwhelming majority of these γδ T cells are naive given their expression of naive marker *SELL* **<Fig 2I,J>**. However, some cells appear to express features of effectorness **<Fig 2K-N>**. This suggests some limitations of transcriptionally driven phenotyping of T cells. Nonetheless, this investigation represents a significant contribution towards deciphering the biology of feline T cells.

192
193 **3.3 Feline circulating T effector cells**
194 As described previously, subtyping T cells with overlapping phenotypes represents a significant
195 challenge, which was further exacerbated by the low number of effector T cells in our dataset.
196 Hence, we clustered effector T cells (clusters 3,4) independently, revealing 13 effector clusters
197 **<Fig3A>**. Many of these clusters represent minimally divergent biological states as reflected by
198 the marked overlap of top differentially expressed genes **<Fig3B, Supplementary File 5>**.
199 However, direct visualization of known phenotypes demonstrate that the effector populations
200 captured exhibit phenotypes of human T_H1, T_H2, T_H17 and T_{reg} cells **<Fig3C-J>** (41,42,44). Gene
201 sets for each module calculation are provided in the supplementary materials **<Supplementary**
202 **file 1, S3>**. These phenotypes do overlap and are not consistent with identified clusters.
203 Nevertheless, the higher scores among closely positioned cells likely indicates the presence of
204 these subtypes. However, a greater sample size of effector cells would be necessary to better
205 resolve subtypes and their trajectory.
206
207 **3.4 Cross species analysis of circulating T cells**
208 To understand how the captured feline T cell populations compared to those of other domestic
209 animal species and humans, we performed an integrative cross-species analysis. We selected 4
210 species for which peer-reviewed annotated scRNA-seq data with over 15,000 cells was available.
211 ScRNA-seq data from three veterinary species (dog, horse and pig) and humans were chosen as
212 the reference for homologous genome mapping (18,21,22,45). In total, we integrated 95,366 cells
213 and identified 13 clusters across the 5 species **<Fig4A-F>**. These clusters were functionally
214 annotated based on markers for T cell identity, naive phenotype, effector phenotype and cytotoxic
215 phenotype in addition to their differential gene expression analysis **<Fig4G,H, Supplementary**
216 **File 6>**.
217
218 Although feline cells were overrepresented in some naive clusters such as 3 and 8, there was
219 limited representation in clusters 5, 6, and 9 particularly **<Fig4I>**. To investigate whether this
220 finding was associated with our enrichment protocol, we assessed *CD5* transcript expression across
221 all clusters **<Fig4J>**. Our results suggest that the number of $CD5^+$ cells and average *CD5*
222 expression were lowest in clusters 5 and 9 **<Fig4K,L>**. Additionally, we saw a direct relationship
223 between the number of feline T cells and the $CD5^+$ cell count in each cluster. Particularly, clusters
224 5, 6, 9, 11, and 12 were most underrepresented **<Fig4M>**. These clusters were identified as
225 cytotoxic effector cells **<Fig4H>**. This highlights a limitation of our CD5 enrichment protocol as
226 it may select against specific effector clusters such as $CD8^+$ cytotoxic cells. Much of our current
227 understanding of $CD8^+$ feline T cells is from flow cytometric studies with no further subtyping
228 due to lack of reagents. Thus, further investigation is necessary to validate whether this low
229 frequency is biological or technical.
230

3.5 V(D)J recombination

To identify patterns in T cell receptor (TR) expression, we sequenced TR alpha (TRA), TR beta (TRB), TR gamma (TRG) and TR delta (TRD) transcripts simultaneously. The majority (>87.0%) of $CD4^+$ naïve, $CD4^+$ T_{EM} and $CD8^+$ naïve T cells expressed TRA/TRB transcripts only **<Fig5A>**. In contrast, only 35.0% of $CD8^+$ cytotoxic T cells expressed TRA/TRB transcripts while 60.6% expressed TRA/TRB/TRG transcripts. γδ T cells primarily expressed TRG/TRD transcripts (49.7%) followed by TRG/TRD/TRB (16.4%) transcripts. Of note, 11.5% of cells had TRA/TRB/TRG transcripts, which might represent αβ T cells with an effector phenotype similar to gd T cells. $CD8^+$ Cytotoxic T cells also exhibited differential TRAV gene usage, and to a lesser degree, TRBV gene usage **<Fig5B,C>**. The junctional length of TRG transcript in $CD8^+$ Cytotoxic T cells was highly skewed towards 16 amino acids and converged on the conserved motif 'CAAWDPRGYGWAHKVF' **<Fig5D>**. Most TRG rearrangements involved cassette 2 (TRGV2-2/TRGJ2-2) **<Fig5E>.** Interestingly, a subset of TRGV2-2 genes rearranged to the TRGJ2-1 gene, which is located upstream of TRGV2-2.

Next, we characterized the repertoire overlap between cats and the relatedness of junctional regions across cats and T cell subsets **<Fig6>**. The number of shared clonotypes was highest for TRA and TRG but overall low **<Fig6A>**. When expanding the definition of shared repertoires to include clonotypes with one amino acid difference, the TRA locus had the highest number, size and publicity of clusters **<Fig6B,C>**.

3.6 Feline circulating monocytic cells

Although $CD5^+$ enrichment was performed for T cell selectivity, we serendipitously captured neutrophils and monocytic cells, which provides insight into the transcriptome of circulating myeloid cells in cats. Clustering analysis of both cell types was performed independently. Due to the low myeloid cell count in the 1YO, it was excluded from this analysis.

Monocytic cells clustered into 5 groups and were largely represented by the 9YO sample **<Fig 7A, Supplementary File 1, S4A>**. Cluster 3 represented neutrophils which is likely due to the close clustering of myeloid cells on the global object **<Fig 1B, Supplementary File 1, S4B>**. Cluster 0, 1 and 2 were identified as classical monocytes (CM) with all clusters having high expression of markers *PLBD1*, *CD83* and classical monocyte markers *CD14* and *VCAN* (28,29,46) **<Fig 7B-D>**. We did not identify any non-classical monocytes, based on absence of *CD16* expression, as seen in other species such as humans, horses and cattle (22,29,46,47). Cluster 4 showed an upregulation of receptor-type tyrosine-protein kinase *FLT3*, a conventional pan-dendritic cell marker (48) **<Fig 7F>**. In addition, these cells exhibited upregulation of MHC class-II molecules (*FECA-DRB*, *HLA-DRA*, *HLA-DOA*, and *HLA-DMD*) and were hence identified as conventional dendritic cells (cDC) (49) **<Fig 7G>**.

In-depth assessment of differentially expressed genes across the four monocytic clusters identified signatures that further characterized these cell types. Cluster 2 demonstrated a proinflammatory phenotype characterized by upregulation of classic proinflammatory cytokines (*IL1A*, *IL1B*), *TNF/NF-KB* pathway (*TNF*, *TNFAIP3, NFKBIA*, *NFKBIZ*, *NFKB1*) and M1-macrophage-associated proinflammatory cytokines (*CXCL10, CXCL16, CCL3, CCL4 and CCL5*) **<Fig 7G,H, Supplementary File 7,8>** (20,50–54). Cluster 1 gene ontology revealed an upregulation of leukocyte migration and chemotaxis terms in addition to upregulation of proinflammatory cytokines *IL1A* and *IL1B* **<Fig 7G,I, Supplementary File 7,8>**. However, these cells also lack *TNF* expression and upregulate anti-inflammatory cytokines *IL10* and *IL18* and proteins which promote anti-inflammatory phenotypes in macrophages such as *LCN2* and *MSRB1* (55,56) **<Fig 7G>**. They have the lowest expression of *CD86*, a T cell co-stimulatory molecule of antigen presenting cells, which is associated with an anti-inflammatory phenotype (57). Most strikingly, these cells were found to upregulate genes similar to a novel monocyte cluster found in SARS-CoV-2 infected and recovered patients. These genes include *AREG*, *EREG*, *BCL6*, *IL10,* and *IL18* which have been described as anti-inflammatory tissue repair genes **<Fig 7G>** (58,59). Thus, these cells were designated as anti-inflammatory, although they do not follow the traditional M2 polarization phenotype described in human monocytes (60). Our data suggests a novel classical monocyte subtype with an anti-inflammatory phenotype.

Cluster 0 (CM) appears the least differentiated with low expression of inflammatory cytokines and the top GO terms include more cellular rather than immune related functions **<Supplementary File 8>**. Cluster 4 (cDC) showed an upregulation of and the GO terms associated with leukocyte activation and T cell activation via TCR contact with antigen bound MHC **<Fig 7G,J, Supplementary File 7,8>**. Given the strong antigen presentation phenotype, the annotation of cDC was further corroborated.

3.7 Feline circulating neutrophils

We identified 2 major neutrophil clusters **<Fig 8A>** based on the expression of canonical neutrophil markers including *CSF3R* and *ELANE* as well as mature neutrophil functional markers vimentin (*VIM)*, thioredoxin (*TXN)*, *S100A9* and *S100A12*, suggesting both clusters are comprised of mature neutrophils (25,61,62) **<Fig 8B-G>**. Cluster 1 exhibited several notable differences compared to cluster 0. Differential gene expression analysis accompanied by gene ontology showed an upregulation in cluster 1 of apoptotic signaling and activated neutrophil functions such as response to lipopolysaccharide and *IL-2* production **<Fig 8H, Supplementary File 9,10>**. Thus, we annotated this cluster as activated neutrophils. When investigating top differentially expressed genes, we noted a higher expression of *IL1A* and *TNFAIP3*, suggesting a proinflammatory phenotype (63) **<Fig 8I,J>**. Similarly, cluster 1 had an increased expression of *VCAN*, which is upregulated in the skin in response to damage from ultraviolet light B and reactive oxygen species (64). Lastly, cluster 1 exhibited lower RNA counts per cell, which is consistent with findings in murine neutrophils where the number of genes and counts of RNA decrease with neutrophil

differentiation, maturation and eventual activation and function (65). Since a pathway driving this clustering could not be resolved, we examined an interferon (IFN) module score, which is a composite score based on expression levels of interferon stimulated genes **<Fig 8N>**. Cluster 1 did not show an increased IFN score but the adjacent cells in cluster 0 did **<Fig 8N>**. Interferon stimulation can delay neutrophil apoptosis, which could represent one of the potential driving factors for cells to move from cluster 0 to cluster 1 (66). This analysis is the first to resolve circulating neutrophil transcriptomic signatures in cats at the single cell level.

4 Discussion

The importance of the cat as a companion animal as well as a model for infectious diseases warrants an in-depth characterization and understanding of the feline immune system. Our study is one of the first to characterize feline immune cell subpopulations at the single cell level. We utilized 5' single cell RNA-sequencing with V(D)J analysis to resolve the heterogeneity of $CD5^+$ enriched peripheral blood immune cells. We resolved populations of T cells, neutrophils, B cells and monocytes. Additionally, this atlas is the first to annotate the single cell transcriptome of rarer cell types, plasmacytoid dendritic cells and mast cells, which are seldomly captured in single cell atlases (67,68).

Among T cells, we were able to resolve different populations of naive cells including a significant number of *CD8A*/*CD8B* naive cells. We further identified T effector cells and terminally differentiated cytotoxic effectors. The transcriptomic gradient of T cell differentiation was found to fit the paradigm seen with other species (23). Additionally, we captured feline γδ T cells for the first time. Upon investigation of effector cells, we were able to demonstrate known T helper effector phenotypes among the most differentiated effectors. Of note, the T_{reg} phenotype was found to be the most prominent. The importance of T_{reg} populations has been studied in cats, particularly in the context of feline mammary carcinoma (69–71). Our study corroborates the large presence of this phenotype and the potential importance of T_{reg} cells in feline immunology.

We performed a cross species integrative analysis of T cells to take advantage of the growing database of single cell RNA data. We found relatively high conservation of T cell subtypes along an effector gradient with relatively equitable representation of veterinary species (horse, dog, pig) and humans with the cat. This analysis also revealed the potential negative impacts of $CD5^+$ enrichment for T cells. Effector clusters with high *CD5* expression were found to be underrepresented in the cat. Thus, a broader T cell selection protocol would be necessary in future studies to further investigate effector cells in cats.

In addition to characterizing T cells based on their transcriptome, we analyzed TCR expression on a single cell level for the first time in the cat. Cytotoxic $CD8^+$ T cells differed from other αβ T cell subsets in multiple aspects. In addition to the expected TRA and TRB transcripts, a high percentage of cytotoxic $CD8^+$ T cells expressed a productive TRG transcript. Given that this was not observed in naïve CD8+ T cells, we attribute this phenomenon to differential transcriptional regulation of

350 naive and effector T cells. Compared to other αβ T cell subsets, cytotoxic T cells also exhibited
351 divergent TRAV and TRBV gene usage but not TRGV gene usage. Instead, the junctional length
352 of TRG transcripts was skewed towards a highly conserved16 aa motif. This finding is of potential
353 significance for clonality testing, an adjunct method for differentiating reactive from neoplastic
354 lymphoid proliferations. If the majority of cytotoxic $CD8^+$ T cells harbor a length restricted TRG
355 rearrangement, then reactive $CD8^+$ dominant T cell proliferations might exhibit reduced TRG
356 diversity, which could result in a higher false positive rate. Of note, since other αβ T cell subsets
357 did not express a significant number of productive TRG transcripts, it is unknown if similar length
358 restricted rearrangements occur in these subsets. A previous study examining the feline TCR
359 transcriptome across thymus, spleen and mesenteric lymph nodes did not identify any TRG length
360 restrictions (13). However, the previous study aimed to identify global rearrangement patterns and
361 hence utilized a bulk sequencing strategy, which is not suited to resolve repertoire characteristics
362 of individual T cell subsets.
363
364 A cluster analysis of TCR sequences did not identify T cell subsets with invariant TRA or TRB
365 chains. A previous study utilizing scRNA-seq with VDJ sequencing in dogs identified MAIT-like
366 cells based on restricted TRAV gene usage and restricted junctional length (19). Although
367 cytotoxic T cells in the present study exhibited differential TRAV gene and, to a lesser extent,
368 differential TRBV gene usage, there was no obvious junctional length restriction or dominant
369 amino acid motif. The fact that we were unable to identify MAIT-like cells in cats could reflect
370 their true absence or represent an artifact of CD5-based enrichment, which might have resulted in
371 the exclusion of $CD5^-$ or $CD5^{low}$ subsets. Additional studies with more animals, inclusion of
372 different tissue types and without selection bias are needed to elucidate the existence of innate-like
373 alpha/beta T cells in cats.
374
375 Among the myeloid cells, we resolved 3 clusters of classical monocytes and 1 cluster of
376 conventional dendritic cells. Of the three clusters of monocytes, we found two to be differentiated
377 in a somewhat polarized manner- pro-inflammatory versus anti-inflammatory. The anti-
378 inflammatory population was unconventional in that it had an upregulation of classic pro-
379 inflammatory cytokines *IL-1A* and IL-*1B* but also an upregulation of genes associated with a
380 unique and novel monocytic cluster found in human COVID-19 patients such as *AREG, EREG,*
381 *IL10* , *IL18* and *BCL6.* (59,72). Sub clustering of neutrophils identified a larger mature cluster and
382 a smaller exhausted/activated cluster which showed upregulation of pro-inflammatory and
383 apoptotic genes. Thus, analysis of these myeloid cells revealed the presence of conventional and
384 non-conventional subtypes, providing a footing for feline circulating myeloid immunology.
385 Currently, T cell subtypes have only been described at the flow cytometric level, and with a focus
386 on *CD4/CD8* populations due to paucity of species-specific reagents. Our data indicates the
387 presence of unique subtypes of peripheral blood immune cells including αβγ $CD8^+$ cytotoxic cells,
388 *CD8A/CD8B* naive T cells, plasmacytoid DC, mast cells, conventional DCs, anti-inflammatory
389 monocytes and mature and end stage neutrophils. Our study is the first of many necessary for the

390 further characterization of the feline immune system. Taken together, it has increased our
391 understanding of feline circulating immune cells, including T cell subtyping and capture of rare
392 populations previously undescribed in the cat.
393
394 **5 Materials and Methods**
395 **5.1 Samples and Sorting**
396 Whole blood was obtained from four healthy, female, domestic shorthair cats (13-101/9 years, 18-
397 003/6 years, 21-005/1 year, 22-007/6 months) housed at the UC Davis Nutrition and Pet Care
398 Center in accordance with the UC Davis Policy and Procedure Manual section 290-30 and Animal
399 Use and Care protocol #22150. Blood was collected in purple top EDTA tubes and immediately
400 processed in one batch without freezing until completion of the reverse transcription step during
401 library preparation. Peripheral blood mononuclear cells (PBMC) were isolated from whole blood
402 by density gravity centrifugation. Briefly, 5 mL of whole blood was layered on top of 10 mL
403 Histopaque 1077 (density 1.077g/mL, Sigma-Aldrich, Burlington, MA, USA) in a 50 ml tube. The
404 samples were centrifuged at 850 revolutions per minute (RCF) for 30 minutes at room temperature
405 (RT) without break. After centrifugation, the PBMC layer at the plasma-histopaque interface was
406 aspirated and transferred to a clean 15 ml tube. The PBMCs were then washed twice with 14 ml
407 PBMC isolation media (500 mL Hanks' Balanced Salt Solution (HBSS), 15 mL Fetal Bovine
408 Serum (FBS), 2 mL EDTA) by centrifuging at 850 RCF for 10 minutes at RT. Following the
409 second washing step, the PBMC pellet was resuspended in 200 µl modified flow buffer solution
410 (MFB, 500 ml phosphate buffer saline (PBS), 0.467g EDTA tetrasodium salt and 1% Horse
411 serum).
412 The isolated PBMCs were first incubated with a primary anti-feline CD5 monoclonal antibody
413 (clone FE 1.1.B11-IgG1-Azide, Peter F. Moore Leukocyte Antigen Biology Laboratory, UC
414 Davis, CA, USA) or a non-cross reacting canine antibody (negative control) for 30 min at RT. This
415 was followed by a wash step (addition off 3 mL of MFB, followed by centrifugation at 400 RCF
416 for 3 min at RT and resuspension in 100 - 200 µl of supernatant), and incubation with a secondary
417 horse-anti-mouse FITC antibody (1:99 in MFB) for 15 minutes at RT in darkness. Finally, the
418 stained PBMC was washed again (as above), resuspended in 500 µl of MFB and stained with DAPI
419 (1 µg/mL). Cells were sorted at the UC Davis Comprehensive Cancer Center Flow Cytometry
420 Core. Cells were initially gated based on FSC vs. SSC to exclude debris and aggregates. Singlet
421 gating was then applied based on SSC to exclude doublets, followed by discrimination of live and
422 dead cells based on DAPI staining and subsequent gating for CD5 positive (FITC positive) cells
423 **<Supplementary File 11>**.
424
425 **5.2 Single-cell 5' RNA and V(D)J library preparation, sequencing and mapping**
426 Libraries were constructed using the Chromium Next GEM Single Cell 5' Kit v2 (10x Genomics).
427 All four feline T cell receptor loci were amplified using the Chromium Single Cell V(D)J
428 Enrichment Kit according to the manufacturer's instructions but with custom reverse primers
429 specific for the feline orthologs **<Supplementary File 12>**. Separate libraries were prepared for

the transcriptome, alpha/beta TCRs, and gamma/delta TCRs **<Supplementary File 12>**. Libraries were sequenced using the Illumina NovaSeq S4 platform using 150 paired-end reads to a target read depth of 30,000 reads per cell. Raw FASTQ sequencing data were processed by the UC Davis Bioinformatics Core using 10X CellRanger version 7.1 for alignment to the cat reference genome (*Felis_catus_9.0*). To improve the quality of annotation of the *Felis catus* genome, we converted unmapped ENSEMBL IDs to human homologs from BioMart for greater interpretative power. Gene mapping was performed in the following order: (1) Mapping of one-to-one orthologs from cat to human (2) Mapping of one-to-many and many-to-many was performed by choosing a representative cat gene based on the following parameters, in respective order [orthology_confidence, gene_order_confidence, Whole_Genome_alignment, %_query_identical_target, %target_identical_query]. Additionally, specific unmapped genes were manually annotated or filtered **<Supplementary File 13>**. Further analysis was then continued using Seurat v5 (73).

5.3 Count matrix pre-processing and quality control

Filtered feature matrices for the 4 samples were independently normalized and scaled using the function *SCTransform* v2 (glmGamPoi) (74). Dimensionality reduction (determined using knee identification in elbow plot), k-means clustering (resolution determined using clustree package) and neighbor identification (74–76) was performed. Low quality clusters were identified and filtered based on low gene counts, high mitochondrial read percentage and lack of biologically relevant markers. To further ensure quality, doublet identification was performed using package *DoubletFinder* according to package vignette and ambient RNA decontamination was performed using the *DecontX* package as per package tutorials adapted to the data (77,78).

5.4 Integration and Downstream analysis

Objects were integrated by sample using the Seurat native reciprocal principal component analysis (RPCA) (79). The embeddings were utilized for Uniform Manifold Approximation and Projection (UMAP) and subsequent clustering and neighbor identification as described prior. Differential gene expression analysis was performed using each cluster identified by the Seurat function *FindAllMarkers* (Non-parametric Wilcoxon Rank Sum with adjusted P value <0.05). Gene set enrichment analyses including over-enrichment analysis (ORA) of gene ontology (biological process) was performed using *ClusterProfiler* on human homologized genes (adjusted P value <0.05) (80). Additional visualizations and associated statistics were performed using ggplot2 and gg supplementary packages (81). Figures were illustrated on Bio Render.

5.5 Cell type sub clustering

Cell type sub-clustering (example: T cell sub-clustering) analysis was performed in the same manner as described prior. Pseudotime values were calculated using the UMAP embeddings produced via Seurat with RPCA integration using package *monocle3* (82). Gene module scores were calculated via the Seurat function *AddModuleScore*.

470
471 **5.6 Cross species T cell integrative analysis**
472 Published single cell RNA-sequencing datasets were obtained from NCBI GEO Accession for 4
473 species including dog (*Canis familiaris*: GSE225599 (18)), human (*Homo sapiens*:
474 https://support.10xgenomics.com/single-cell-gene-expression/datasets/3.0.0/pbmc_10k_v3),
475 horse (*Equus caballus*: GSE148416 (22)) and pig (*Sus*
476 *scrofa*: https://data.nal.usda.gov/dataset/data-reference-transcriptomics-porcine-peripheral-
477 immune-cells-created-through-bulk-and-single-cell-rna-sequencing. (21)). All species genes were
478 mapped to human homologs as described prior for the cat. Only homologized shared genes
479 between all 5 species were utilized for analysis. T cell clusters annotated by authors were validated
480 using canonical T cell markers (*CD3E*, *CD3D*, *TCF7*, *LCK*, *ITK*). T cells were integrated across
481 species using Seurat canonical correlation analysis (CCA) and downstream analysis proceeded in
482 the same manner as described prior for global object analysis.
483
484 **5.7 VDJ analysis**
485 Contigs were mapped to available IMGT reference genes (as of February 2023) using Cell Ranger
486 version 7.1. All analyses were based on the 'all_contig_annotations.csv' file using the R packages
487 tidyverse, circlize and ggseqlogo (83-85). Cluster analysis was performed as previously described
488 (86).
489
490 **5.8 Data availability**
491 All raw and processed data have been submitted to NCBI GEO and are available under
492 GSE267355.
493
494 **6 Acknowledgements**
495 This project was funded by grant #2022-24-F from the Center for Companion Animal Health,
496 University of California, Davis. The project was supported by the University of California Davis
497 Flow Cytometry Shared Resource Laboratory with funding from the NCI P30 CA093373
498 (Comprehensive Cancer Center) and S10 OD018223, with technical assistance from Bridget
499 McLaughlin, Jonathan Van Dyke and Ashley Karajeh. The sequencing was carried out by the
500 DNA Technologies and Expression Analysis Core at the UC Davis Genome Center, supported
501 by NIH Shared Instrumentation Grant 1S10OD010786-01. We thank Jie (Jessie) Li from the UC
502 Davis Bioinformatics Core for data analysis and Kristy Harmon from the Leukocyte Biology
503 Antigen Laboratory for her flow cytometry support.
504
505
506 **7 References**
507 1. Rowan AN. Companion Animal Statistics in the USA. 2018 [cited 2024 Apr 30];
508 Available from: https://www.wellbeingintlstudiesrepository.org/demscapop/7/

2. Larkin M, Radich R. AVMA. Am Vet Med Assoc; 2021 [cited 2024 Apr 5]. Pet population still on the rise, with fewer pets per household. Available from: https://avmajournals.avma.org/display/post/news/pet-population-still-on-the-rise--with-fewer-pets-per-household.xml?print&print&print&print&print
3. Fromont E, Artois M, Langlais M, Courchamp F, Pontier D. Modelling the feline leukemia virus (FeLV) in natural populations of cats (Felis catus). Theor Popul Biol [Internet]. 1997 Aug;52(1):60–70. Available from: http://dx.doi.org/10.1006/tpbi.1997.1320
4. Powers JA, Chiu ES, Kraberger SJ, Roelke-Parker M, Lowery I, Erbeck K, et al. Feline Leukemia Virus (FeLV) Disease Outcomes in a Domestic Cat Breeding Colony: Relationship to Endogenous FeLV and Other Chronic Viral Infections. J Virol [Internet]. 2018 Sep 15;92(18). Available from: http://dx.doi.org/10.1128/JVI.00649-18
5. Helfer-Hungerbuehler AK, Shah J, Meili T, Boenzli E, Li P, Hofmann-Lehmann R. Adeno-Associated Vector-Delivered CRISPR/SaCas9 System Reduces Feline Leukemia Virus Production In Vitro. Viruses [Internet]. 2021 Aug 18;13(8). Available from: http://dx.doi.org/10.3390/v13081636
6. Bienzle D. FIV in cats--a useful model of HIV in people? Vet Immunol Immunopathol [Internet]. 2014 Jun 15;159(3-4):171–9. Available from: http://dx.doi.org/10.1016/j.vetimm.2014.02.014
7. Paillot R, Richard S, Bloas F, Piras F, Poulet H, Brunet S, et al. Toward a detailed characterization of feline immunodeficiency virus-specific T cell immune responses and mediated immune disorders. Vet Immunol Immunopathol [Internet]. 2005 Jun 15;106(1-2):1–14. Available from: http://dx.doi.org/10.1016/j.vetimm.2004.12.023
8. Endo Y, Matsumura S, Washizu T, Ishida T. Alteration of T-cell subsets in the lymph nodes from cats infected with feline immunodeficiency virus. J Vet Med Sci [Internet]. 1997 Sep;59(9):739–46. Available from: http://dx.doi.org/10.1292/jvms.59.739
9. Hoffmann-Fezer G, Mortelbauer W, Hartmann K, Mysliwietz J, Thefeld S, Beer B, et al. Comparison of T-cell subpopulations in cats naturally infected with feline leukaemia virus or feline immunodeficiency virus. Res Vet Sci [Internet]. 1996 Nov;61(3):222–6. Available from: http://dx.doi.org/10.1016/s0034-5288(96)90067-3
10. Day MJ. Cats are not small dogs: is there an immunological explanation for why cats are less affected by arthropod-borne disease than dogs? Parasit Vectors [Internet]. 2016 Sep 20;9(1):507. Available from: http://dx.doi.org/10.1186/s13071-016-1798-5
11. Akira S, Uematsu S, Takeuchi O. Pathogen recognition and innate immunity. Cell [Internet]. 2006 Feb 24;124(4):783–801. Available from: http://dx.doi.org/10.1016/j.cell.2006.02.015
12. Jiao A, Zhang C, Wang X, Sun L, Liu H, Su Y, et al. Single-cell sequencing reveals the evolution of immune molecules across multiple vertebrate species. J Advert Res [Internet]. 2023 Mar 4; Available from: http://dx.doi.org/10.1016/j.jare.2023.02.017

548 13. Radtanakatikanon A, Keller SM, Darzentas N, Moore PF, Folch G, Nguefack Ngoune V,
549 et al. Topology and expressed repertoire of the Felis catus T cell receptor loci. BMC
550 Genomics [Internet]. 2020 Jan 6;21(1):20. Available from:
551 http://dx.doi.org/10.1186/s12864-019-6431-5
552 14. Ginhoux F, Yalin A, Dutertre CA, Amit I. Single-cell immunology: Past, present, and
553 future. Immunity [Internet]. 2022 Mar 8;55(3):393–404. Available from:
554 http://dx.doi.org/10.1016/j.immuni.2022.02.006
555 15. Jovic D, Liang X, Zeng H, Lin L, Xu F, Luo Y. Single-cell RNA sequencing
556 technologies and applications: A brief overview. Clin Transl Med [Internet]. 2022
557 Mar;12(3):e694. Available from:
558 https://onlinelibrary.wiley.com/doi/abs/10.1002/ctm2.694
559 16. Sun X, Lin X, Li Z, Wu H. A comprehensive comparison of supervised and unsupervised
560 methods for cell type identification in single-cell RNA-seq. Brief Bioinform [Internet].
561 2022 Mar 10;23(2). Available from: http://dx.doi.org/10.1093/bib/bbab567
562 17. Wang M, Song WM, Ming C, Wang Q, Zhou X, Xu P, et al. Guidelines for
563 bioinformatics of single-cell sequencing data analysis in Alzheimer's disease: review,
564 recommendation, implementation and application. Mol Neurodegener [Internet]. 2022
565 Mar 2;17(1):17. Available from: http://dx.doi.org/10.1186/s13024-022-00517-z
566 18. Ammons DT, Harris RA, Hopkins LS, Kurihara J, Weishaar K, Dow S. A single-cell
567 RNA sequencing atlas of circulating leukocytes from healthy and osteosarcoma affected
568 dogs. Front Immunol [Internet]. 2023 May 19;14:1162700. Available from:
569 http://dx.doi.org/10.3389/fimmu.2023.1162700
570 19. Eschke M, Moore PF, Chang H, Alber G, Keller SM. Canine peripheral blood TCRαβ T
571 cell atlas: Identification of diverse subsets including CD8A+ MAIT-like cells by
572 combined single-cell transcriptome and V(D)J repertoire analysis. Front Immunol
573 [Internet]. 2023 Feb 23;14:1123366. Available from:
574 http://dx.doi.org/10.3389/fimmu.2023.1123366
575 20. Gao Y, Li J, Cai G, Wang Y, Yang W, Li Y, et al. Single-cell transcriptomic and
576 chromatin accessibility analyses of dairy cattle peripheral blood mononuclear cells and
577 their responses to lipopolysaccharide. BMC Genomics [Internet]. 2022 Apr 30;23(1):338.
578 Available from: http://dx.doi.org/10.1186/s12864-022-08562-0
579 21. Herrera-Uribe J, Wiarda JE, Sivasankaran SK, Daharsh L, Liu H, Byrne KA, et al.
580 Reference Transcriptomes of Porcine Peripheral Immune Cells Created Through Bulk
581 and Single-Cell RNA Sequencing. Front Genet [Internet]. 2021 Jun 23;12:689406.
582 Available from: http://dx.doi.org/10.3389/fgene.2021.689406
583 22. Patel RS, Tomlinson JE, Divers TJ, Van de Walle GR, Rosenberg BR. Single-cell
584 resolution landscape of equine peripheral blood mononuclear cells reveals diverse cell
585 types including T-bet+ B cells. BMC Biol [Internet]. 2021 Jan 22;19(1):13. Available
586 from: http://dx.doi.org/10.1186/s12915-020-00947-5

587 23. Li Z, Sun C, Wang F, Wang X, Zhu J, Luo L, et al. Molecular mechanisms governing
588 circulating immune cell heterogeneity across different species revealed by single-cell
589 sequencing. Clin Transl Med [Internet]. 2022 Jan;12(1):e689. Available from:
590 http://dx.doi.org/10.1002/ctm2.689
591 24. Touw IP, Palande K, Beekman R. Granulocyte colony-stimulating factor receptor
592 signaling: implications for G-CSF responses and leukemic progression in severe
593 congenital neutropenia. Hematol Oncol Clin North Am [Internet]. 2013 Feb;27(1):61–73,
594 viii. Available from: http://dx.doi.org/10.1016/j.hoc.2012.10.002
595 25. Sprenkeler EGG, Zandstra J, van Kleef ND, Goetschalckx I, Verstegen B, Aarts CEM, et
596 al. S100A8/A9 Is a Marker for the Release of Neutrophil Extracellular Traps and Induces
597 Neutrophil Activation. Cells [Internet]. 2022 Jan 11;11(2). Available from:
598 http://dx.doi.org/10.3390/cells11020236
599 26. Akgun E, Tuzuner MB, Sahin B, Kilercik M, Kulah C, Cakiroglu HN, et al. Proteins
600 associated with neutrophil degranulation are upregulated in nasopharyngeal swabs from
601 SARS-CoV-2 patients. PLoS One [Internet]. 2020 Oct 20;15(10):e0240012. Available
602 from: http://dx.doi.org/10.1371/journal.pone.0240012
603 27. Blanter M, Cambier S, De Bondt M, Vanbrabant L, Pörtner N, Abouelasrar Salama S, et
604 al. Method Matters: Effect of Purification Technology on Neutrophil Phenotype and
605 Function. Front Immunol [Internet]. 2022 Feb 10;13:820058. Available from:
606 http://dx.doi.org/10.3389/fimmu.2022.820058
607 28. Buechler C, Ritter M, Orsó E, Langmann T, Klucken J, Schmitz G. Regulation of
608 scavenger receptor CD163 expression in human monocytes and macrophages by pro- and
609 antiinflammatory stimuli. J Leukoc Biol [Internet]. 2000 Jan;67(1):97–103. Available
610 from: https://www.ncbi.nlm.nih.gov/pubmed/10648003
611 29. Sampath P, Moideen K, Ranganathan UD, Bethunaickan R. Monocyte Subsets:
612 Phenotypes and Function in Tuberculosis Infection. Front Immunol [Internet]. 2018 Jul
613 30;9:1726. Available from: http://dx.doi.org/10.3389/fimmu.2018.01726
614 30. Reshetnikova E, Guselnikov S, Volkova O, Baranov K, Taranin A, Mechetina L. B cell-
615 specific protein FCRLA is expressed by plasmacytoid dendritic cells in humans.
616 Cytometry B Clin Cytom [Internet]. 2018 Jul;94(4):683–7. Available from:
617 http://dx.doi.org/10.1002/cyto.b.21611
618 31. Rissoan MC, Duhen T, Bridon JM, Bendriss-Vermare N, Péronne C, de Saint Vis B, et
619 al. Subtractive hybridization reveals the expression of immunoglobulin-like transcript 7,
620 Eph-B1, granzyme B, and 3 novel transcripts in human plasmacytoid dendritic cells.
621 Blood [Internet]. 2002 Nov 1;100(9):3295–303. Available from:
622 http://dx.doi.org/10.1182/blood-2002-02-0638
623 32. Edwards AD, Diebold SS, Slack EMC, Tomizawa H, Hemmi H, Kaisho T, et al. Toll-like
624 receptor expression in murine DC subsets: lack of TLR7 expression by CD8α+ DC
625 correlates with unresponsiveness to imidazoquinolines. Eur J Immunol [Internet]. 2003

Apr;33(4):827–33. Available from: https://onlinelibrary.wiley.com/doi/10.1002/eji.200323797

33. Medina KL, Tangen SN, Seaburg LM, Thapa P, Gwin KA, Shapiro VS. Separation of plasmacytoid dendritic cells from B-cell-biased lymphoid progenitor (BLP) and Pre-pro B cells using PDCA-1. PLoS One [Internet]. 2013 Oct 30;8(10):e78408. Available from: http://dx.doi.org/10.1371/journal.pone.0078408

34. Arroyo Hornero R, Idoyaga J. Plasmacytoid dendritic cells: A dendritic cell in disguise. Mol Immunol [Internet]. 2023 Jul;159:38–45. Available from: http://dx.doi.org/10.1016/j.molimm.2023.05.007

35. Atiakshin D, Kostin A, Trotsenko I, Samoilova V, Buchwalow I, Tiemann M. Carboxypeptidase A3-A Key Component of the Protease Phenotype of Mast Cells. Cells [Internet]. 2022 Feb 6;11(3). Available from: http://dx.doi.org/10.3390/cells11030570

36. Cruse G, Kaur D, Leyland M, Bradding P. A novel FcεRIβ-chain truncation regulates human mast cell proliferation and survival. FASEB J [Internet]. 2010 Oct;24(10):4047–57. Available from: http://dx.doi.org/10.1096/fj.10-158378

37. Lee H, Joo JY, Kang J, Yu Y, Kim YH, Park HR. Single-cell analysis of platelets from patients with periodontitis and diabetes. Res Pract Thromb Haemost [Internet]. 2023 Feb;7(2):100099. Available from: http://dx.doi.org/10.1016/j.rpth.2023.100099

38. Yang S, Liu F, Wang QJ, Rosenberg SA, Morgan RA. The shedding of CD62L (L-selectin) regulates the acquisition of lytic activity in human tumor reactive T lymphocytes. PLoS One [Internet]. 2011 Jul 28;6(7):e22560. Available from: http://dx.doi.org/10.1371/journal.pone.0022560

39. Ivetic A, Hoskins Green HL, Hart SJ. L-selectin: A Major Regulator of Leukocyte Adhesion, Migration and Signaling. Front Immunol [Internet]. 2019 May 14;10:1068. Available from: http://dx.doi.org/10.3389/fimmu.2019.01068

40. Bjorkdahl O, Barber KA, Brett SJ, Daly MG, Plumpton C, Elshourbagy NA, et al. Characterization of CC-chemokine receptor 7 expression on murine T cells in lymphoid tissues. Immunology [Internet]. 2003 Oct;110(2):170–9. Available from: http://dx.doi.org/10.1046/j.1365-2567.2003.01727.x

41. Cano-Gamez E, Soskic B, Roumeliotis TI, So E, Smyth DJ, Baldrighi M, et al. Single-cell transcriptomics identifies an effectorness gradient shaping the response of CD4+ T cells to cytokines. Nat Commun [Internet]. 2020 Apr 14;11(1):1801. Available from: http://dx.doi.org/10.1038/s41467-020-15543-y

42. Zhu J, Yamane H, Paul WE. Differentiation of Effector CD4 T Cell Populations*. Annu Rev Immunol [Internet]. 2009 Apr 23 [cited 2024 Mar 23];28(Volume 28, 2009):445–89. Available from: https://www.annualreviews.org/content/journals/10.1146/annurev-immunol-030409-101212

43. Andreatta M, Corria-Osorio J, Müller S, Cubas R, Coukos G, Carmona SJ. Interpretation of T cell states from single-cell transcriptomics data using reference atlases. Nat

Commun [Internet]. 2021 May 20;12(1):2965. Available from: http://dx.doi.org/10.1038/s41467-021-23324-4

44. Wang X, Shen X, Chen S, Liu H, Hong N, Zhong H, et al. Reinvestigation of Classic T Cell Subsets and Identification of Novel Cell Subpopulations by Single-Cell RNA Sequencing. J Immunol [Internet]. 2022 Jan 15;208(2):396–406. Available from: http://dx.doi.org/10.4049/jimmunol.2100581

45. Vallejo J, Saigusa R, Gulati R, Armstrong Suthahar SS, Suryawanshi V, Alimadadi A, et al. Combined protein and transcript single-cell RNA sequencing in human peripheral blood mononuclear cells. BMC Biol [Internet]. 2022 Sep 1;20(1):193. Available from: http://dx.doi.org/10.1186/s12915-022-01382-4

46. Schneider L, Marcondes NA, Hax V, da Silva Moreira IF, Ueda CY, Piovesan RR, et al. Flow cytometry evaluation of CD14/CD16 monocyte subpopulations in systemic sclerosis patients: a cross sectional controlled study. Adv Rheumatol [Internet]. 2021 May 22;61(1):27. Available from: http://dx.doi.org/10.1186/s42358-021-00182-8

47. Barut GT, Kreuzer M, Bruggmann R, Summerfield A, Talker SC. Single-cell transcriptomics reveals striking heterogeneity and functional organization of dendritic and monocytic cells in the bovine mesenteric lymph node. Front Immunol [Internet]. 2022;13:1099357. Available from: http://dx.doi.org/10.3389/fimmu.2022.1099357

48. Waskow C, Liu K, Darrasse-Jèze G, Guermonprez P, Ginhoux F, Merad M, et al. The receptor tyrosine kinase Flt3 is required for dendritic cell development in peripheral lymphoid tissues. Nat Immunol [Internet]. 2008 Jun;9(6):676–83. Available from: http://dx.doi.org/10.1038/ni.1615

49. ten Broeke T, Wubbolts R, Stoorvogel W. MHC class II antigen presentation by dendritic cells regulated through endosomal sorting. Cold Spring Harb Perspect Biol [Internet]. 2013 Dec 1;5(12):a016873. Available from: http://dx.doi.org/10.1101/cshperspect.a016873

50. Eislmayr K, Bestehorn A, Morelli L, Borroni M, Vande Walle L, Lamkanfi M, et al. Nonredundancy of IL-1α and IL-1β is defined by distinct regulation of tissues orchestrating resistance versus tolerance to infection. Sci Adv [Internet]. 2022 Mar 4;8(9):eabj7293. Available from: http://dx.doi.org/10.1126/sciadv.abj7293

51. Lopez-Castejon G, Brough D. Understanding the mechanism of IL-1β secretion. Cytokine Growth Factor Rev [Internet]. 2011 Aug;22(4):189–95. Available from: http://dx.doi.org/10.1016/j.cytogfr.2011.10.001

52. Hadadi E, Zhang B, Baidžajevas K, Yusof N, Puan KJ, Ong SM, et al. Differential IL-1β secretion by monocyte subsets is regulated by Hsp27 through modulating mRNA stability. Sci Rep [Internet]. 2016 Dec 15;6:39035. Available from: http://dx.doi.org/10.1038/srep39035

53. Wan J, Shan Y, Fan Y, Fan C, Chen S, Sun J, et al. NF-κB inhibition attenuates LPS-induced TLR4 activation in monocyte cells. Mol Med Rep [Internet]. 2016 Nov;14(5):4505–10. Available from: http://dx.doi.org/10.3892/mmr.2016.5825

705 54. Mussbacher M, Derler M, Basílio J, Schmid JA. NF-κB in monocytes and macrophages -
706 an inflammatory master regulator in multitalented immune cells. Front Immunol
707 [Internet]. 2023 Feb 23;14:1134661. Available from:
708 http://dx.doi.org/10.3389/fimmu.2023.1134661
709 55. Guo H, Jin D, Chen X. Lipocalin 2 is a regulator of macrophage polarization and NF-
710 κB/STAT3 pathway activation. Mol Endocrinol [Internet]. 2014 Oct;28(10):1616–28.
711 Available from: http://dx.doi.org/10.1210/me.2014-1092
712 56. Lee BC, Lee SG, Choo MK, Kim JH, Lee HM, Kim S, et al. Selenoprotein MsrB1
713 promotes anti-inflammatory cytokine gene expression in macrophages and controls
714 immune response in vivo. Sci Rep [Internet]. 2017 Jul 11;7(1):5119. Available from:
715 http://dx.doi.org/10.1038/s41598-017-05230-2
716 57. Vishnyakova P, Poltavets A, Karpulevich E, Maznina A, Vtorushina V, Mikhaleva L, et
717 al. The response of two polar monocyte subsets to inflammation. Biomed Pharmacother
718 [Internet]. 2021 Jul;139:111614. Available from:
719 http://dx.doi.org/10.1016/j.biopha.2021.111614
720 58. Zhang Y, Wang S, Xia H, Guo J, He K, Huang C, et al. Identification of Monocytes
721 Associated with Severe COVID-19 in the PBMCs of Severely Infected Patients Through
722 Single-Cell Transcriptome Sequencing. Engineering [Internet]. 2022 Oct;17:161–9.
723 Available from: http://dx.doi.org/10.1016/j.eng.2021.05.009
724 59. Utrero-Rico A, González-Cuadrado C, Chivite-Lacaba M, Cabrera-Marante O, Laguna-
725 Goya R, Almendro-Vazquez P, et al. Alterations in Circulating Monocytes Predict
726 COVID-19 Severity and Include Chromatin Modifications Still Detectable Six Months
727 after Recovery. Biomedicines [Internet]. 2021 Sep 17;9(9). Available from:
728 http://dx.doi.org/10.3390/biomedicines9091253
729 60. Rynikova M, Adamkova P, Hradicka P, Stofilova J, Harvanova D, Matejova J, et al.
730 Transcriptomic Analysis of Macrophage Polarization Protocols: Vitamin D3 or IL-4 and
731 IL-13 Do Not Polarize THP-1 Monocytes into Reliable M2 Macrophages. Biomedicines
732 [Internet]. 2023 Feb 17;11(2). Available from:
733 http://dx.doi.org/10.3390/biomedicines11020608
734 61. Wigerblad G, Cao Q, Brooks S, Naz F, Gadkari M, Jiang K, et al. Single-Cell Analysis
735 Reveals the Range of Transcriptional States of Circulating Human Neutrophils. J
736 Immunol [Internet]. 2022 Aug 15;209(4):772–82. Available from:
737 http://dx.doi.org/10.4049/jimmunol.2200154
738 62. Meng Y, Lin S, Niu K, Ma Z, Lin H, Fan H. Vimentin affects inflammation and
739 neutrophil recruitment in airway epithelium during Streptococcus suis serotype 2
740 infection. Vet Res [Internet]. 2023 Jan 30;54(1):7. Available from:
741 http://dx.doi.org/10.1186/s13567-023-01135-3
742 63. McColl SR, Paquin R, Ménard C, Beaulieu AD. Human neutrophils produce high levels
743 of the interleukin 1 receptor antagonist in response to granulocyte/macrophage colony-

stimulating factor and tumor necrosis factor alpha. J Exp Med [Internet]. 1992 Aug 1;176(2):593–8. Available from: http://dx.doi.org/10.1084/jem.176.2.593

64. Kunisada M, Yogianti F, Sakumi K, Ono R, Nakabeppu Y, Nishigori C. Increased expression of versican in the inflammatory response to UVB- and reactive oxygen species-induced skin tumorigenesis. Am J Pathol [Internet]. 2011 Dec;179(6):3056–65. Available from: http://dx.doi.org/10.1016/j.ajpath.2011.08.042

65. Xie X, Shi Q, Wu P, Zhang X, Kambara H, Su J, et al. Single-cell transcriptome profiling reveals neutrophil heterogeneity in homeostasis and infection. Nat Immunol [Internet]. 2020 Sep;21(9):1119–33. Available from: http://dx.doi.org/10.1038/s41590-020-0736-z

66. Glennon-Alty L, Moots RJ, Edwards SW, Wright HL. Type I interferon regulates cytokine-delayed neutrophil apoptosis, reactive oxygen species production and chemokine expression. Clin Exp Immunol [Internet]. 2021 Feb;203(2):151–9. Available from: http://dx.doi.org/10.1111/cei.13525

67. Leylek R, Idoyaga J. Chapter Four - The versatile plasmacytoid dendritic cell: Function, heterogeneity, and plasticity. In: Lhuillier C, Galluzzi L, editors. International Review of Cell and Molecular Biology [Internet]. Academic Press; 2019. p. 177–211. Available from: https://www.sciencedirect.com/science/article/pii/S1937644819300991

68. Varricchi G, de Paulis A, Marone G, Galli SJ. Future Needs in Mast Cell Biology. Int J Mol Sci [Internet]. 2019 Sep 6;20(18). Available from: http://dx.doi.org/10.3390/ijms20184397

69. Nascimento C, Ferreira F. Tumor microenvironment of human breast cancer, and feline mammary carcinoma as a potential study model. Biochim Biophys Acta Rev Cancer [Internet]. 2021 Aug;1876(1):188587. Available from: http://dx.doi.org/10.1016/j.bbcan.2021.188587

70. Andrade LM, Sousa ECM, Melo ACS, Pardavil GSS, Silva RA, Valente KF, et al. Gene expression of cytokines in the blood of domestics cats infected and not infected by Feline alphaherpesvirus. Available from: http://dx.doi.org/10.4238/gmr19190

71. Smithberg SR, Fogle JE, Mexas AM, Reckling SK, Lankford SM, Tompkins MB, et al. In vivo depletion of CD4+CD25+ regulatory T cells in cats. J Immunol Methods [Internet]. 2008 Jan 1;329(1-2):81–91. Available from: http://dx.doi.org/10.1016/j.jim.2007.09.015

72. Rigamonti A, Castagna A, Viatore M, Colombo FS, Terzoli S, Peano C, et al. Distinct responses of newly identified monocyte subsets to advanced gastrointestinal cancer and COVID-19. Front Immunol [Internet]. 2022 Oct 3;13:967737. Available from: http://dx.doi.org/10.3389/fimmu.2022.967737

73. Satija R, Farrell JA, Gennert D, Schier AF, Regev A. Spatial reconstruction of single-cell gene expression data. Nat Biotechnol [Internet]. 2015 May;33(5):495–502. Available from: http://dx.doi.org/10.1038/nbt.3192

74. Hafemeister C, Satija R. Normalization and variance stabilization of single-cell RNA-seq data using regularized negative binomial regression. Genome Biol [Internet]. 2019 Dec 23;20(1):296. Available from: http://dx.doi.org/10.1186/s13059-019-1874-1
75. Zappia L, Oshlack A. Clustering trees: a visualization for evaluating clusterings at multiple resolutions. Gigascience [Internet]. 2018 Jul 1;7(7). Available from: http://dx.doi.org/10.1093/gigascience/giy083
76. Ahlmann-Eltze C, Huber W. glmGamPoi: fitting Gamma-Poisson generalized linear models on single cell count data. Bioinformatics [Internet]. 2021 Apr 5;36(24):5701–2. Available from: http://dx.doi.org/10.1093/bioinformatics/btaa1009
77. Yang S, Corbett SE, Koga Y, Wang Z, Johnson WE, Yajima M, et al. Decontamination of ambient RNA in single-cell RNA-seq with DecontX. Genome Biol [Internet]. 2020 Mar 5;21(1):57. Available from: http://dx.doi.org/10.1186/s13059-020-1950-6
78. McGinnis CS, Murrow LM, Gartner ZJ. DoubletFinder: Doublet Detection in Single-Cell RNA Sequencing Data Using Artificial Nearest Neighbors. Cell Syst [Internet]. 2019 Apr 24;8(4):329–37.e4. Available from: http://dx.doi.org/10.1016/j.cels.2019.03.003
79. Song Y, Miao Z, Brazma A, Papatheodorou I. Benchmarking strategies for cross-species integration of single-cell RNA sequencing data. Nat Commun [Internet]. 2023 Oct 14;14(1):6495. Available from: http://dx.doi.org/10.1038/s41467-023-41855-w
80. Wu T, Hu E, Xu S, Chen M, Guo P, Dai Z, et al. clusterProfiler 4.0: A universal enrichment tool for interpreting omics data. Innovation (Camb) [Internet]. 2021 Aug 28;2(3):100141. Available from: http://dx.doi.org/10.1016/j.xinn.2021.100141
81. Wickham H. ggplot2 [Internet]. Springer International Publishing; [cited 2023 Oct 16]. 16 p. Available from: https://link.springer.com/book/10.1007/978-3-319-24277-4
82. Trapnell C, Cacchiarelli D, Grimsby J, Pokharel P, Li S, Morse M, et al. The dynamics and regulators of cell fate decisions are revealed by pseudotemporal ordering of single cells. Nat Biotechnol [Internet]. 2014 Apr;32(4):381–6. Available from: http://dx.doi.org/10.1038/nbt.2859
83. R Core Team (2023). _R: A Language and Environment for Statistical Computing_. R Foundation for Statistical Computing, Vienna, Austria. <https://www.R-project.org/>.
84. Gu Z, Gu L, Eils R, Schlesner M, Brors B. circlize Implements and enhances circular visualization in R. Bioinformatics. 2014 Oct;30(19):2811-2. doi: 10.1093/bioinformatics/btu393. Epub 2014 Jun 14. PMID: 24930139.
85. Wickham H, Averick M, Bryan J, Chang W, McGowan LD, François R, Grolemund G, Hayes A, Henry L, Hester J, Kuhn M, Pedersen TL, Miller E, Bache SM, Müller K, Ooms J, Robinson D, Seidel DP, Spinu V, Takahashi K, Vaughan D, Wilke C, Woo K, Yutani H (2019). “Welcome to the tidyverse.” Journal of Open Source Software, 4(43), 1686. doi:10.21105/joss.01686.

86. Chang H, Ashlock DA, Graether SP, Keller SM. Anchor Clustering for million-scale immune repertoire sequencing data. BMC Bioinformatics. 2024 Jan 25;25(1):42. doi: 10.1186/s12859-024-05659-z. PMID: 38273275; PMCID: PMC10809746.

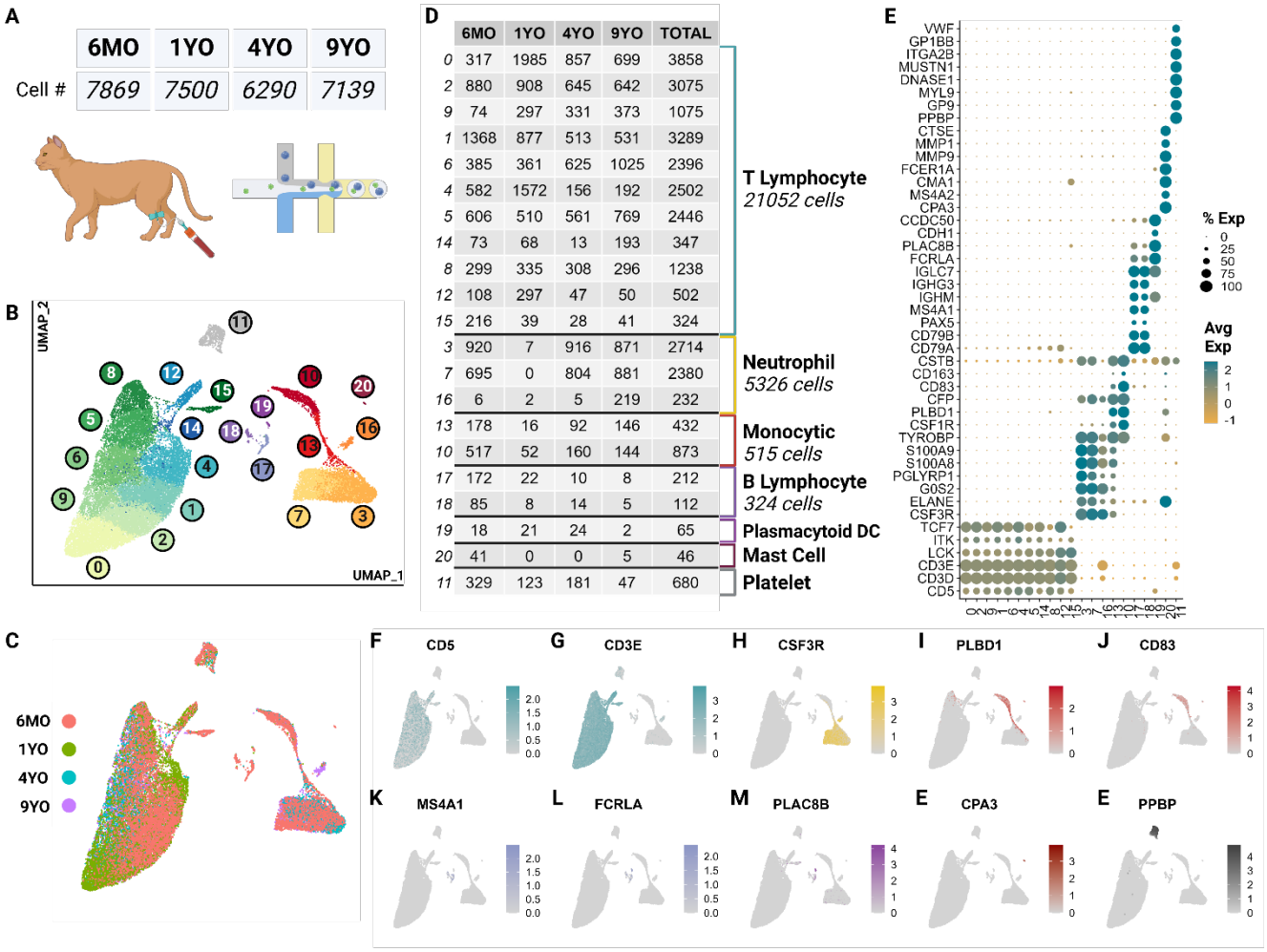

Figure 1. scRNA-seq atlas of CD5^{+} enriched circulating feline immune cells revealed 7 major types across 21 clusters. (A) Table of cell counts from each age group. (B) UMAP plot demonstrating the unsupervised clustering results for feline circulating immune cells from 4 healthy cats of different age groups. (C) UMAP plot of global clustering colored by age. (D) Table of cell type counts across clusters by age. (E) Dot plot demonstrating cell type specific marker expression of the 7 major cell types. (F-O) Feature UMAP plots demonstrating expression profile of key markers for each of the 7 different cell types.

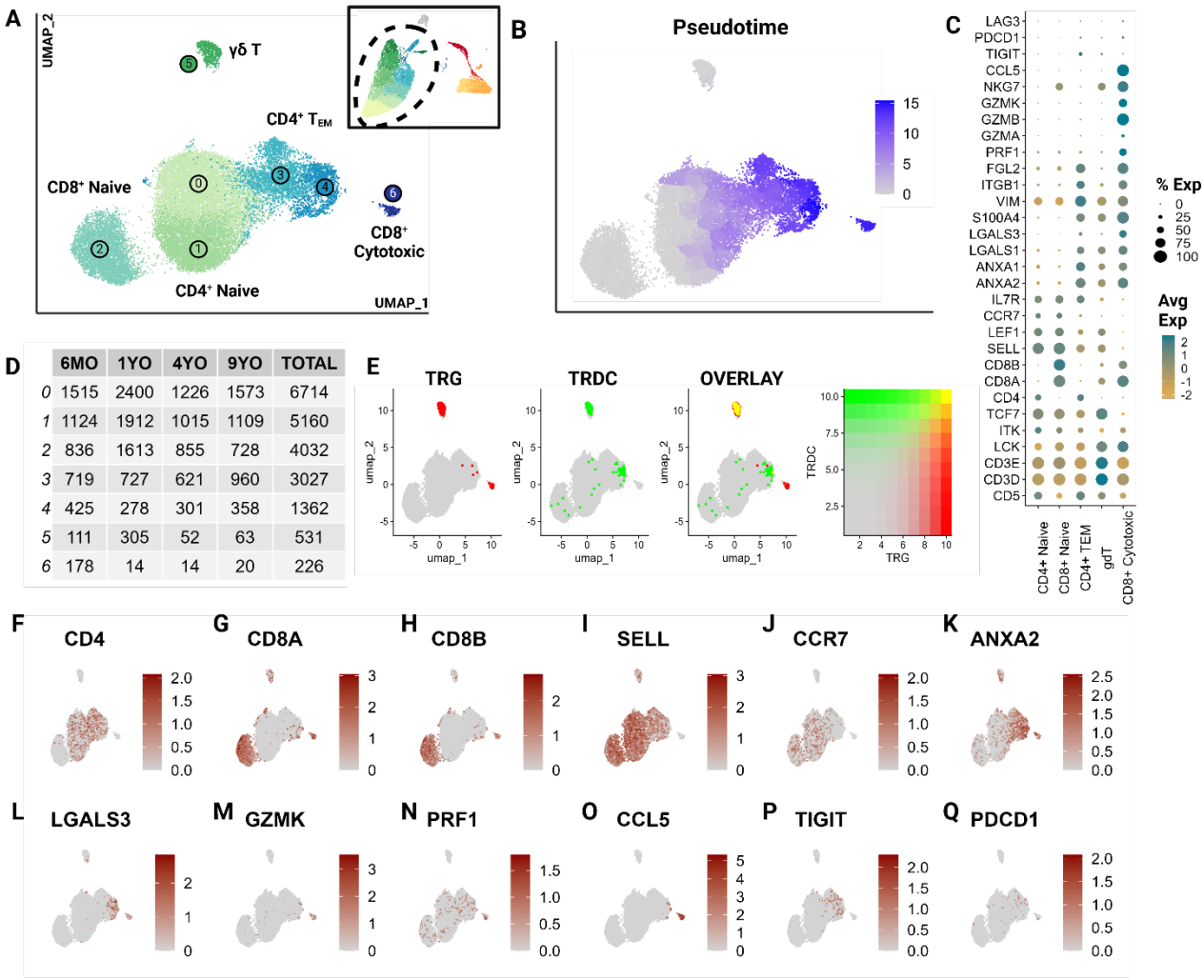

	6MO	1YO	4YO	9YO	TOTAL
0	1515	2400	1226	1573	6714
1	1124	1912	1015	1109	5160
2	836	1613	855	728	4032
3	719	727	621	960	3027
4	425	278	301	358	1362
5	111	305	52	63	531
6	178	14	14	20	226

Figure 2. CD5^{+} enriched T cells segregate into naïve T cell subtypes and effectors. Unsupervised clustering of T cells reveals 7 subtypes. (A) UMAP of the scRNA-seq atlas of T cells. (B) UMAP of T cells colored by Pseudotime. (C) Dot plot of marker genes expressed by T cell type. (D) Table of cell type frequencies across ages by cluster. (E) Feature plots of expression and co-expression of *TRG* and *TRDC*. (F-Q) UMAP of T cells colored by classical T marker genes defining *CD4*/*CD8* status, naive (*SELL*, *CCR7*), effectorness (*ANXA2*, *LGALS3*, *GZMK, PRF1*), terminal differentiation (CCL5) and T exhaustion (*TIGIT*, *PDCD1*).

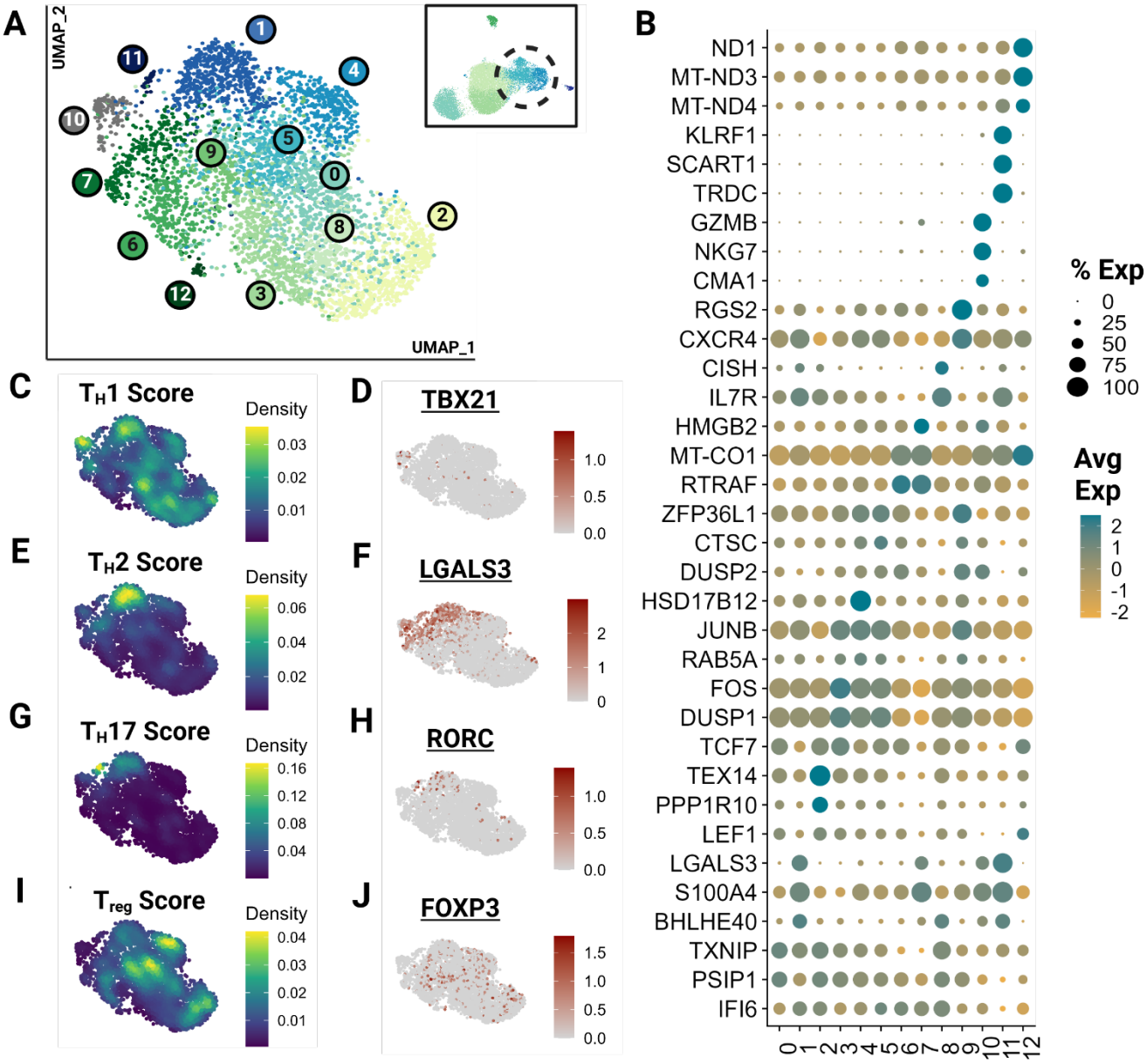

Figure 3. Feline Effector T cells (T_{EM}) segregate into transcriptionally similar clusters and reveal the presence of helper T phenotypes. Unsupervised clustering of T_{EM} reveals 13 subtypes. (A) UMAP of scRNA-seq atlas of T_{EM}. (B) Dot plot demonstrating up to 3 top differentially expressed genes for each cluster determined via Wilcoxon rank sum testing (*Adj P <0.05*). (C,E,G,I) UMAP of T_{EM} colored by helper T subtype gene modules. (D,F,H,J) Expression UMAP of a representative gene from each helper T gene module presented in parallel.

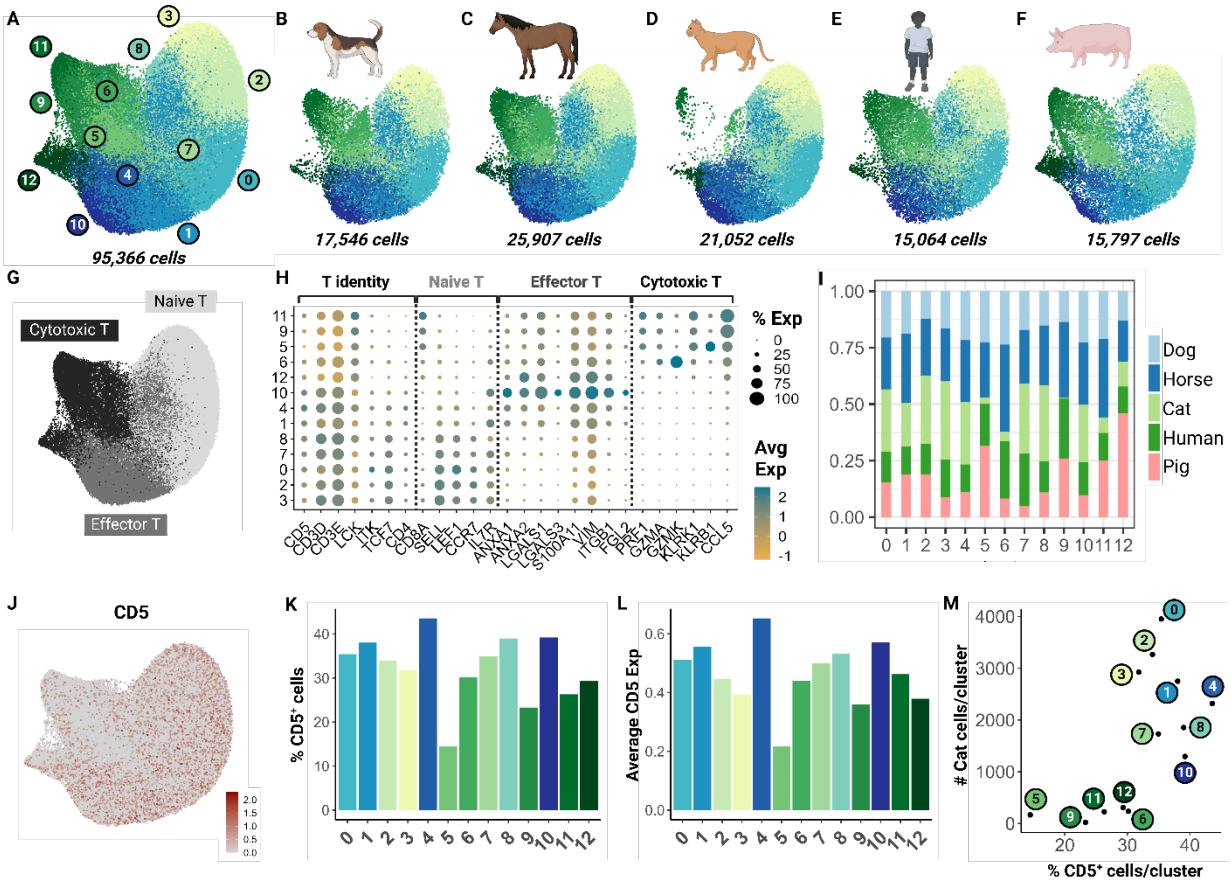

Figure 4. Cross-species integrative analysis of T cells reveals missing cytotoxic effectors in the cat. Unsupervised clustering revealed 12 clusters across 5 species. (A) UMAP of scRNA-seq atlas of T cells. (B-F) UMAP split by species- dog, horse, cat, human and pig. (G) UMAP of T cells colored by T cell phenotype. (H) Dot plot of marker gene sets for T cell subtypes. (I) Percentage bar chart of clusters stacked by species. (J) UMAP colored by *CD5* expression. (K) Bar chart of percentage *CD5*$^{+}$ cells per cluster. (L) Bar chart of average *CD5* expression across cells in each cluster. (M) Scatter plot of percentage *CD5*$^{+}$ cells per cluster versus number of cat cells within the corresponding cluster.

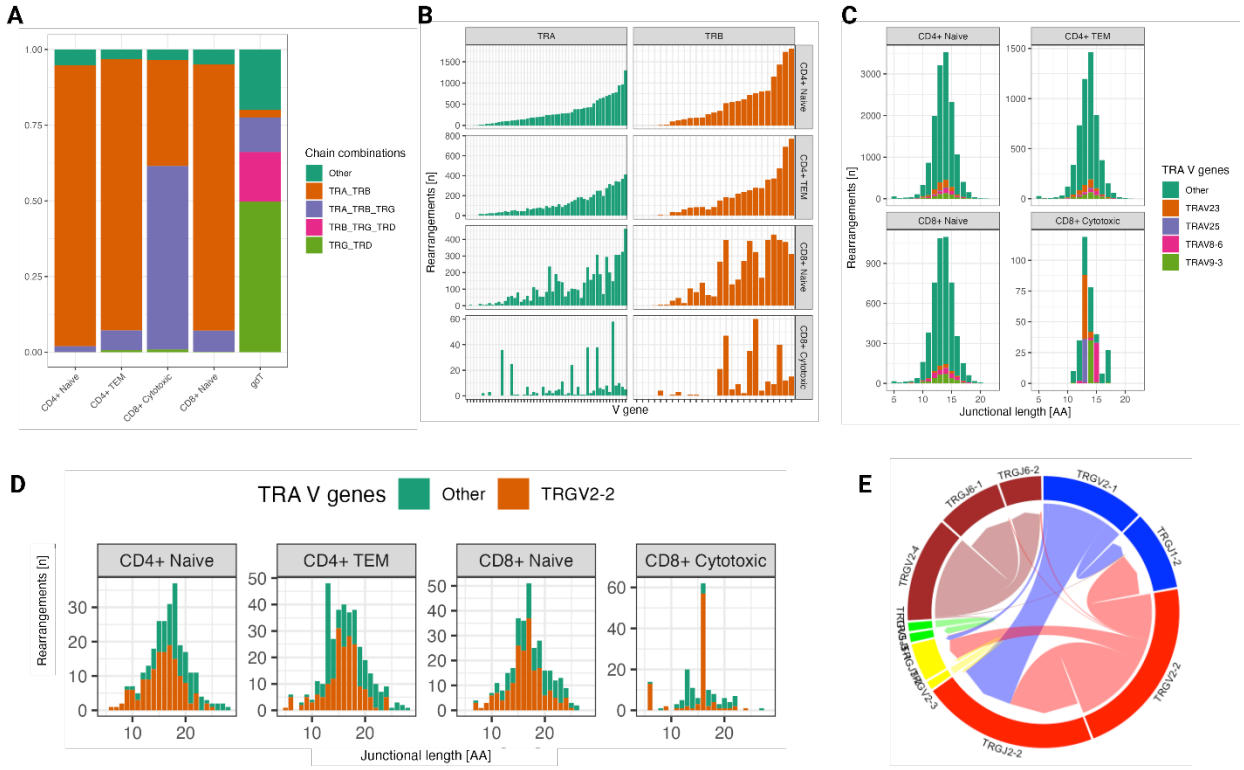

Figure 5. (A) Percentage of T cells expressing a certain combination of productive TR chain transcripts. TRA/TRB transcripts dominate in all ab T cell subsets except for CD8$^+$ cytotoxic T cells, which primarily express TRA/TRB/TRG transcripts. (B) TRA & TRB V gene usage of the 4 major ab T cell subsets. CD8$^+$ cytotoxic T cells show differential usage compared to the other T cell subset but are also substantiated by fewer cells. (C) Junctional length of TRA rearrangements of the 4 major ab T cell subsets. Junctional regions with dominant TRAV genes in CD8$^+$ cytotoxic T cells are 13 and 14 amino acids long. (D) TRG transcripts in CD8$^+$ cytotoxic T cells have a skewed junctional length with 16 amino acid length (top) and a conserved motif (bottom) (E) The majority of TRG rearrangements in CD8$^+$ cytotoxic T cells involved cassette 2 (TRGV2-2/TRGJ2-2). Genes are displayed in order of genomic location and colored by cassette.

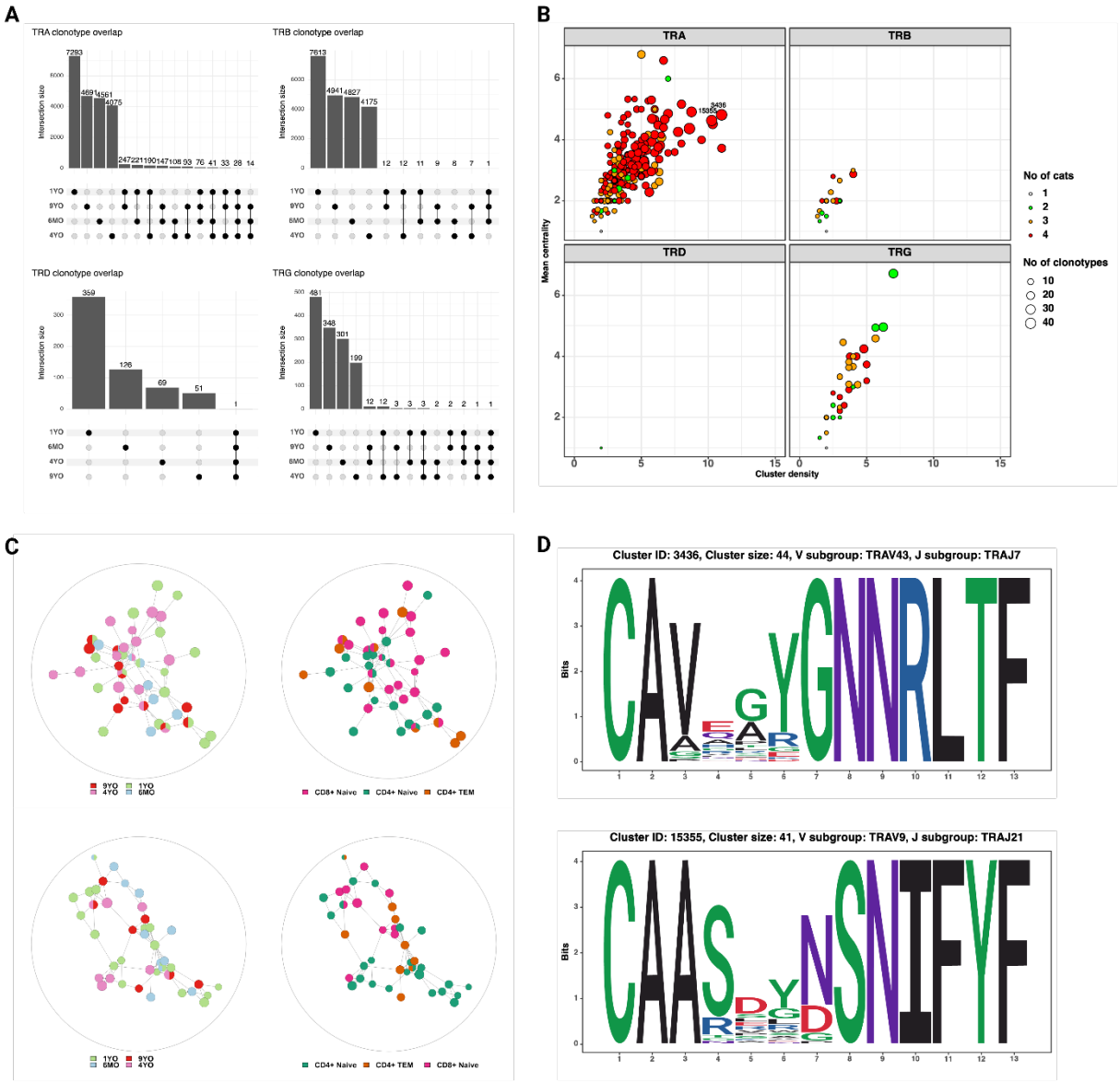

Figure 6. (A) Shared clonotypes across 4 cats. (B) Characterization of clusters based on mean centrality and cluster density. (C) Representative examples of TRA clusters with high centrality and density.

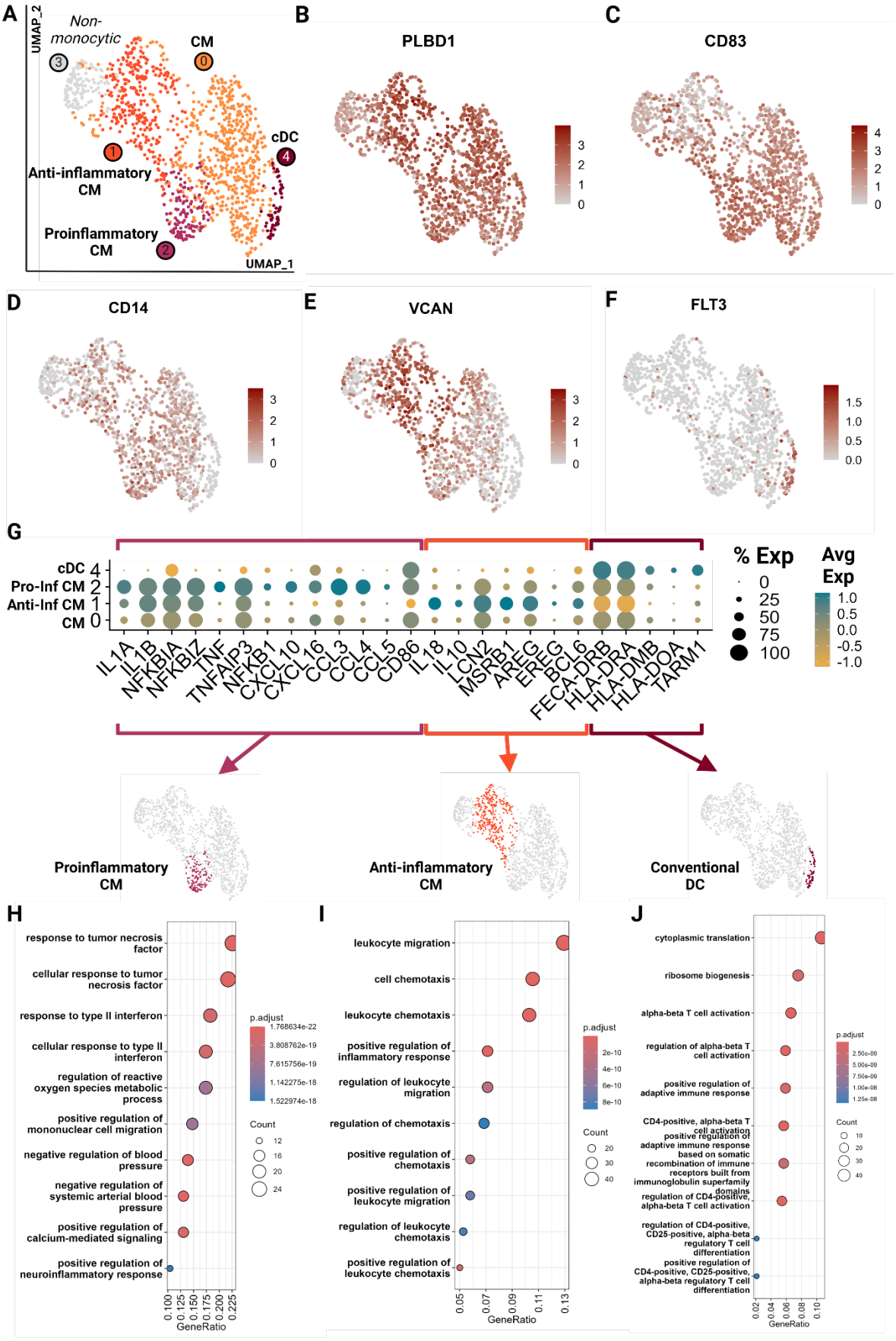
A
UMAP_2
Non-monocytic
CM
cDC
Anti-inflammatory CM
Proinflammatory CM
UMAP_1
B
PLBD1
C
CD83
D
CD14
E
VCAN
F
FLT3
G
cDC
Pro-Inf CM
Anti-Inf CM
CM
IL1A
IL1B
NFKBIA
NFKBIZ
TNF
TNFAIP3
NFKB1
CXCL10
CXCL16
CCL3
CCL4
CCL5
CD86
IL18
IL10
LCN2
MSRB1
AREG
EREG
BCL6
FECA-DRB
HLA-DRA
HLA-DMB
HLA-DOA
TARM1
% Exp
Avg Exp
Proinflammatory CM
Anti-inflammatory CM
Conventional DC
H
response to tumor necrosis factor
cellular response to tumor necrosis factor
response to type II interferon
cellular response to type II interferon
regulation of reactive oxygen species metabolic process
positive regulation of mononuclear cell migration
negative regulation of blood pressure
negative regulation of systemic arterial blood pressure
positive regulation of calcium-mediated signaling
positive regulation of neuroinflammatory response
GeneRatio
p.adjust
Count
I
leukocyte migration
cell chemotaxis
leukocyte chemotaxis
positive regulation of inflammatory response
regulation of leukocyte migration
regulation of chemotaxis
positive regulation of chemotaxis
positive regulation of leukocyte migration
regulation of leukocyte chemotaxis
positive regulation of leukocyte chemotaxis
GeneRatio
p.adjust
Count
J
cytoplasmic translation
ribosome biogenesis
alpha-beta T cell activation
regulation of alpha-beta T cell activation
positive regulation of adaptive immune response
CD4-positive, alpha-beta T cell activation
positive regulation of adaptive immune response based on somatic recombination of immune receptors built from immunoglobulin superfamily domains
regulation of CD4-positive, alpha-beta T cell activation
regulation of CD4-positive, CD25-positive, alpha-beta regulatory T cell differentiation
positive regulation of CD4-positive, CD25-positive, alpha-beta regulatory T cell differentiation
GeneRatio
p.adjust
Count

878 **Figure 7.** Feline circulating monocytes include classical monocytes with more differentiated
879 clusters with traditional proinflammatory and unconventional anti-inflammatory phenotypes.
880 Unsupervised clustering revealed 5 clusters. (A) UMAP of scRNA-seq atlas of monocytes. (B-
881 F) UMAP of monocytes colored by expression levels of canonical markers. (G) Dot plot of
882 genes of monocytic phenotypes across the 4 monocytic clusters. (H-J) Dot plots of top GO
883 biological process terms called based on sets of positive differentially expressed genes
884 identified via Seurat *FindMarker* function (Wilcoxon rank sum, *Adj P <0.05*). Classical
885 monocyte, CM; Conventional dendritic cell, cDC; Pro-inf, proinflammatory; Anti-inf, anti-
886 inflammatory.

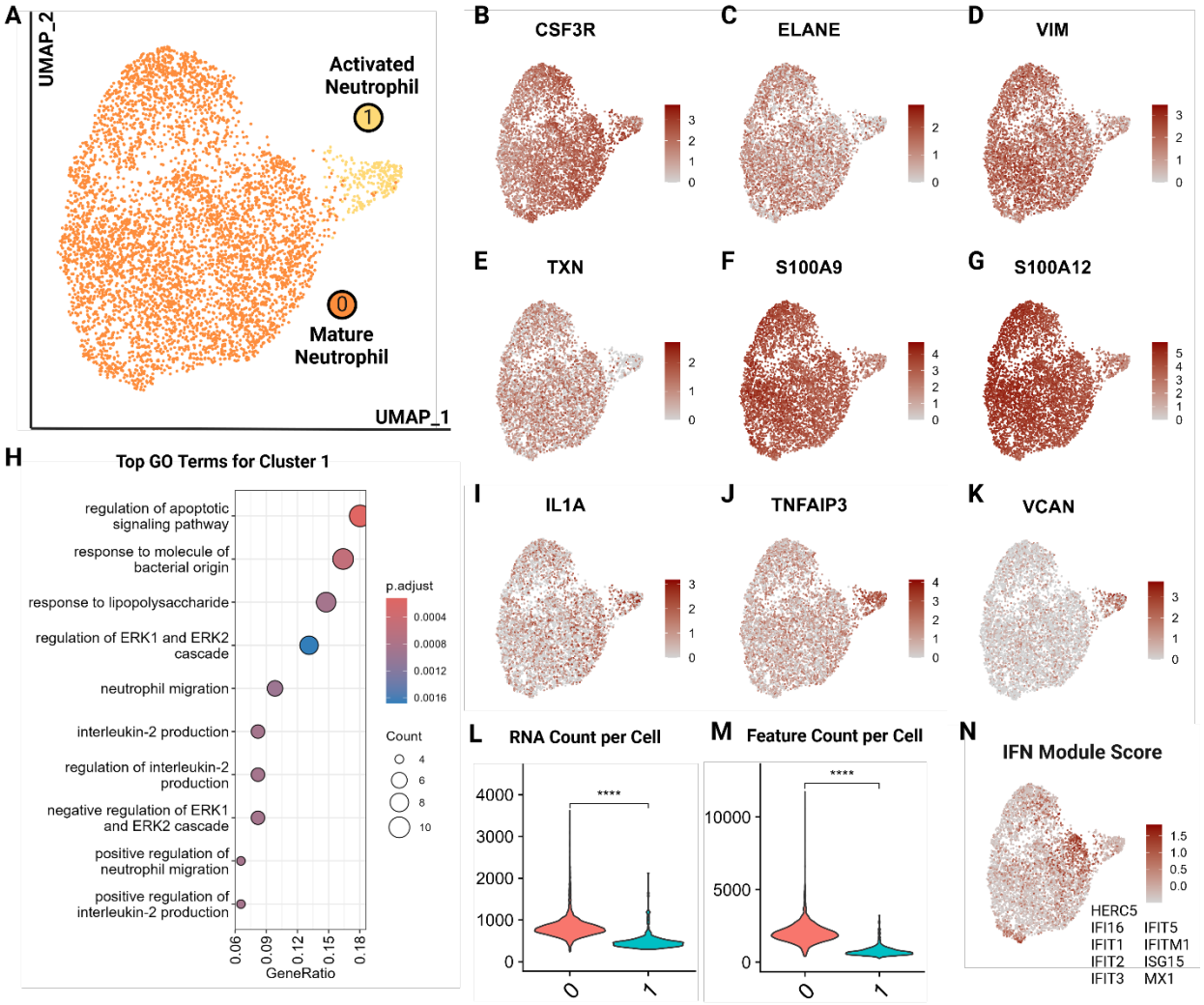

Figure 8. Feline circulating neutrophils separate into 2 clusters based on activation state. (A) UMAP of scRNA-seq atlas of neutrophils. (B-G) UMAP of neutrophils colored by expression levels of canonical and functional neutrophil markers. (H) Dot plots of top GO biological process terms in cluster 1 called based on sets of positive differentially expressed genes identified via Seurat *FindMarker* function (Wilcoxon rank sum, Adj $P < 0.05$). (I-K) UMAP of neutrophils colored by expression levels of select differentially upregulated genes in cluster 1. (L,M) Violin plots of RNA counts and feature (unique RNA) counts per cell by cluster; (****) indicates P value less than 0.001 by T-test. (N) UMAP of neutrophils colored by interferon (IFN) gene composite score per cell; genes included are named in figure.

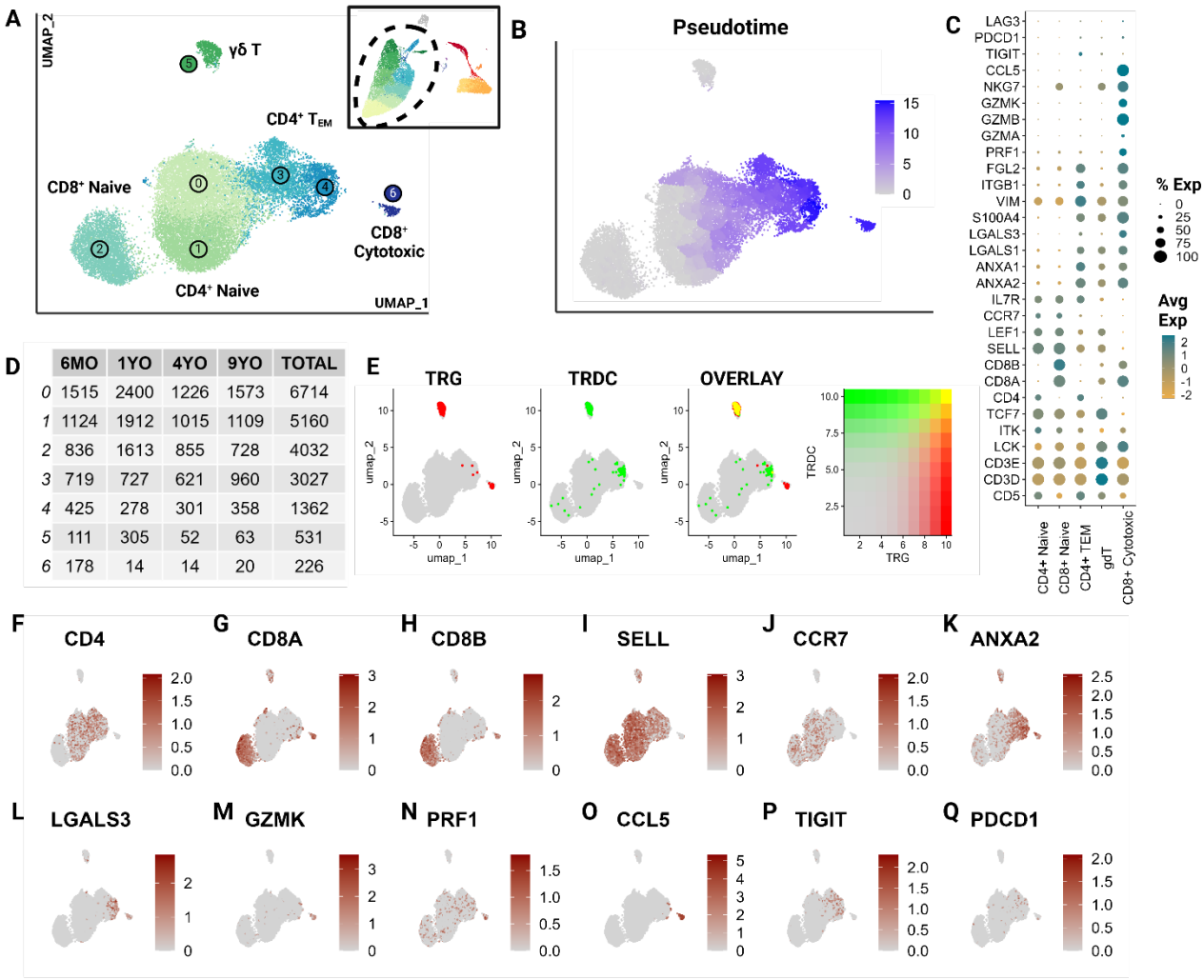

	6MO	1YO	4YO	9YO	TOTAL
0	1515	2400	1226	1573	6714
1	1124	1912	1015	1109	5160
2	836	1613	855	728	4032
3	719	727	621	960	3027
4	425	278	301	358	1362
5	111	305	52	63	531
6	178	14	14	20	226

Figure 2. CD5^{+} enriched T cells segregate into naïve T cell subtypes and effectors. Unsupervised clustering of T cells reveals 7 subtypes. (A) UMAP of the scRNA-seq atlas of T cells. (B) UMAP of T cells colored by Pseudotime. (C) Dot plot of marker genes expressed by T cell type. (D) Table of cell type frequencies across ages by cluster. (E) Feature plots of expression and co-expression of *TRG* and *TRDC*. (F-Q) UMAP of T cells colored by classical T marker genes defining *CD4*/*CD8* status, naive (*SELL*, *CCR7*), effectorness (*ANXA2*, *LGALS3*, *GZMK, PRF1*), terminal differentiation (CCL5) and T exhaustion (*TIGIT*, *PDCD1*).

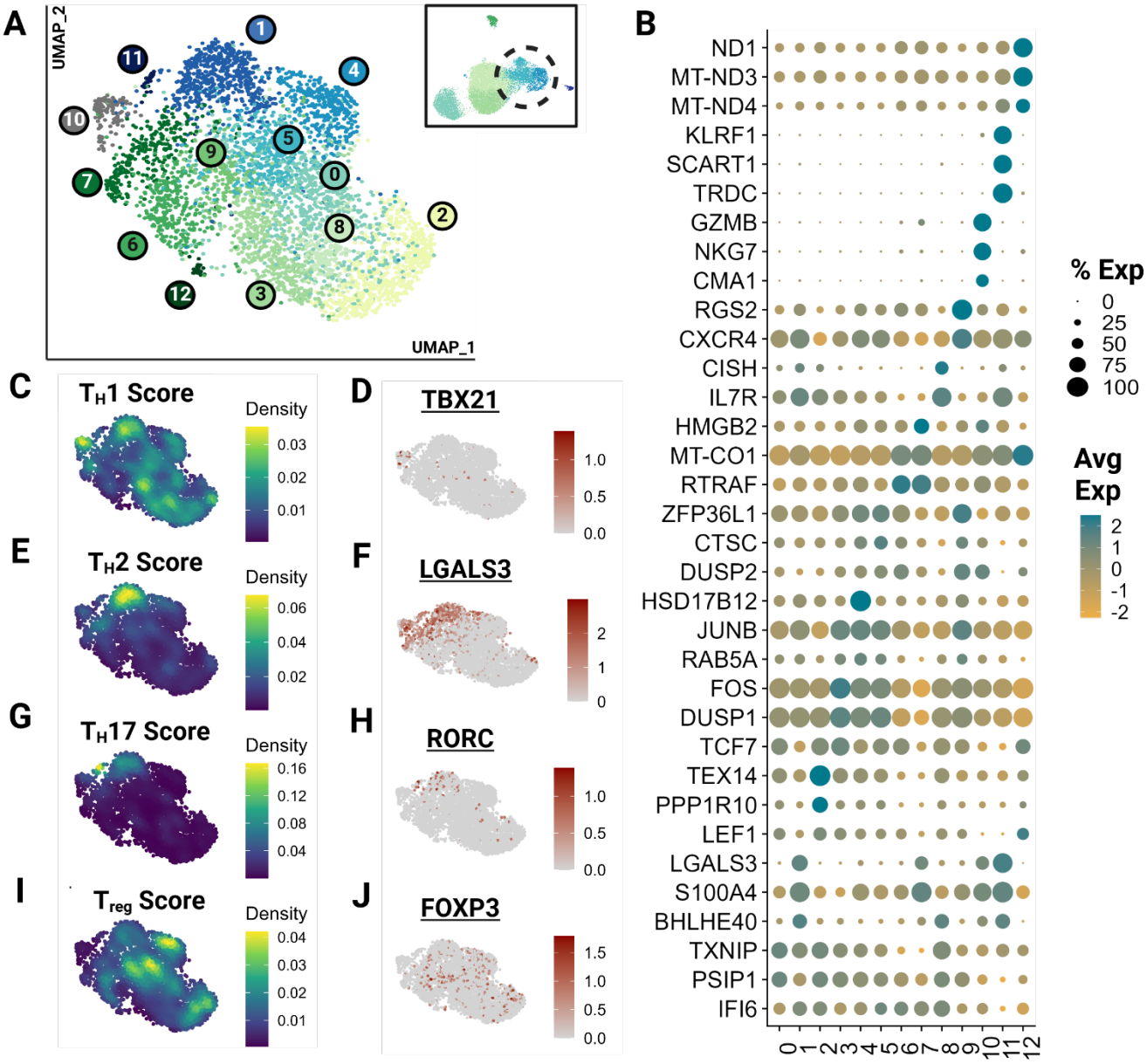

Figure 3. Feline Effector T cells (T_{EM}) segregate into transcriptionally similar clusters and reveal the presence of helper T phenotypes. Unsupervised clustering of T_{EM} reveals 13 subtypes. (A) UMAP of scRNA-seq atlas of T_{EM}. (B) Dot plot demonstrating up to 3 top differentially expressed genes for each cluster determined via Wilcoxon rank sum testing (*Adj P <0.05*). (C,E,G,I) UMAP of T_{EM} colored by helper T subtype gene modules. (D,F,H,J) Expression UMAP of a representative gene from each helper T gene module presented in parallel.

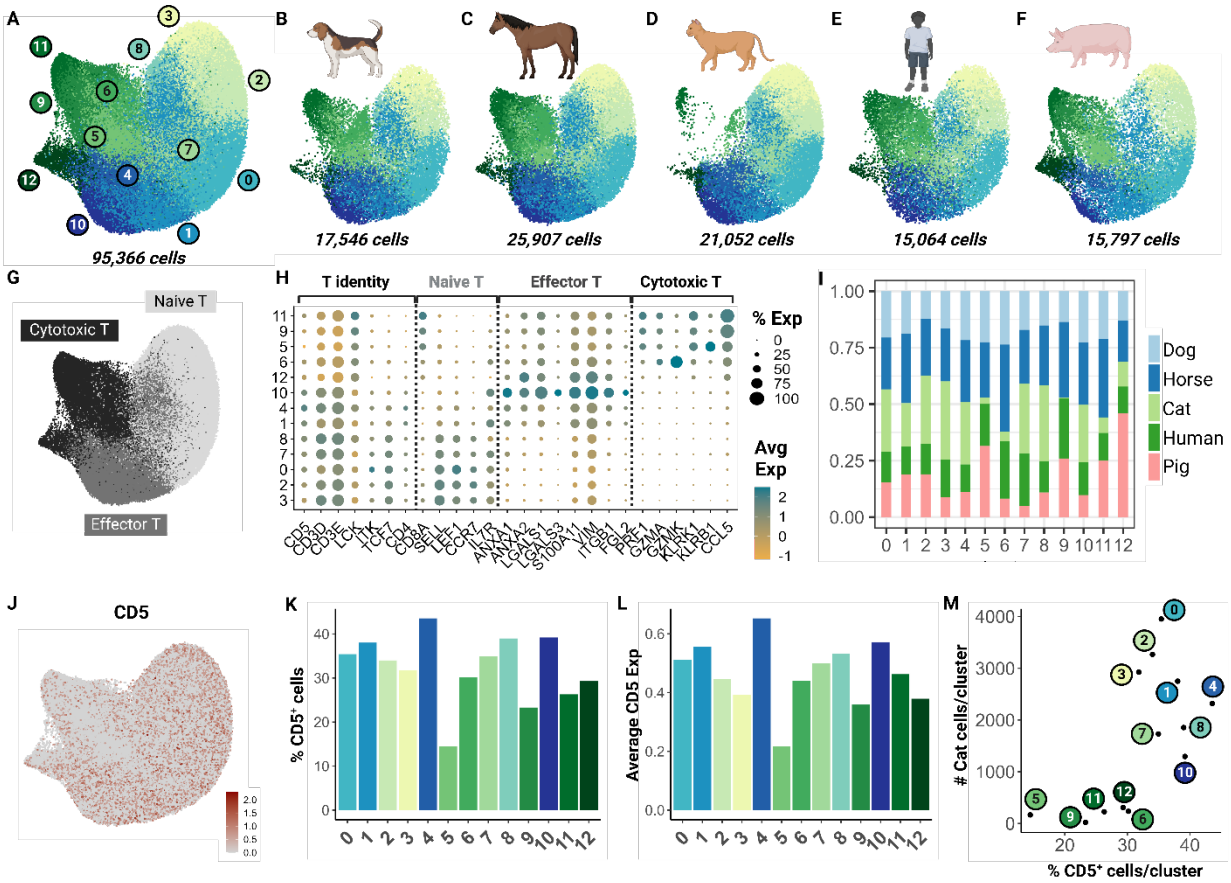

Figure 4. Cross-species integrative analysis of T cells reveals missing cytotoxic effectors in the cat. Unsupervised clustering revealed 12 clusters across 5 species. (A) UMAP of scRNA-seq atlas of T cells. (B-F) UMAP split by species- dog, horse, cat, human and pig. (G) UMAP of T cells colored by T cell phenotype. (H) Dot plot of marker gene sets for T cell subtypes. (I) Percentage bar chart of clusters stacked by species. (J) UMAP colored by *CD5* expression. (K) Bar chart of percentage *CD5*$^{+}$ cells per cluster. (L) Bar chart of average *CD5* expression across cells in each cluster. (M) Scatter plot of percentage *CD5*$^{+}$ cells per cluster versus number of cat cells within the corresponding cluster.

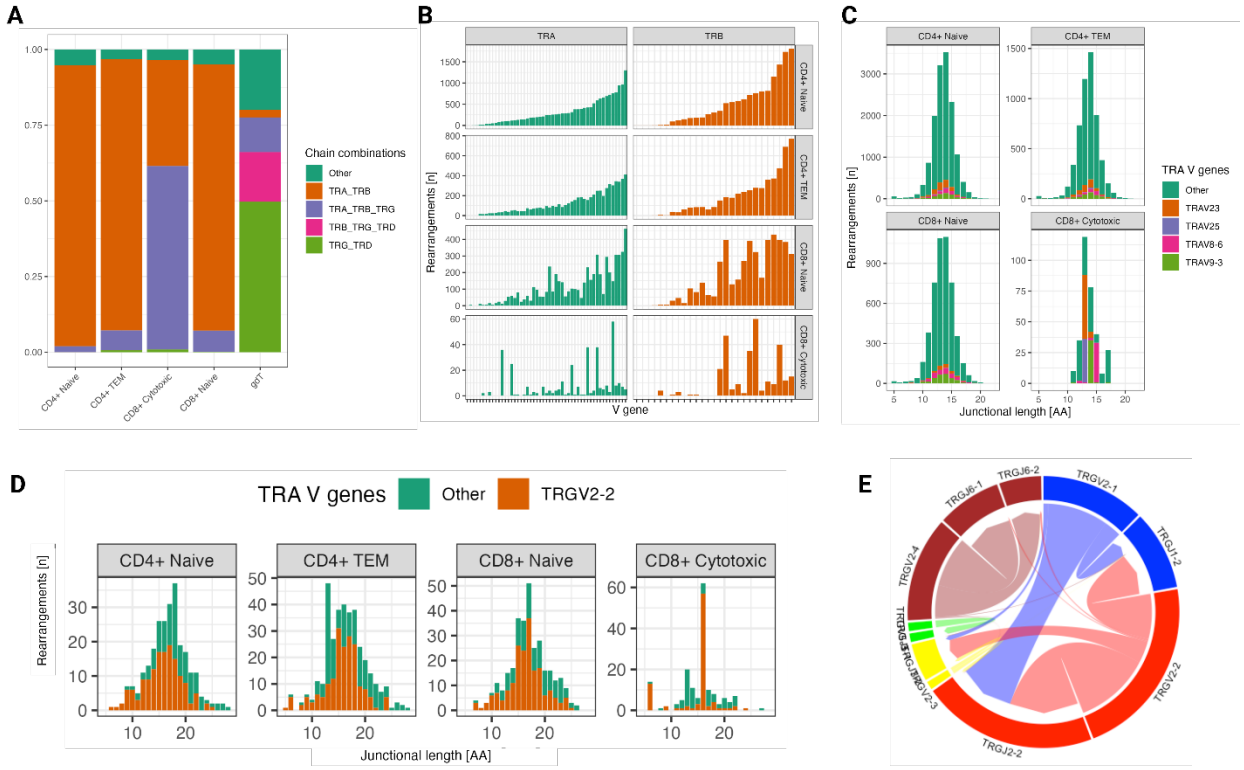

Figure 5. (A) Percentage of T cells expressing a certain combination of productive TR chain transcripts. TRA/TRB transcripts dominate in all ab T cell subsets except for CD8$^+$ cytotoxic T cells, which primarily express TRA/TRB/TRG transcripts. (B) TRA & TRB V gene usage of the 4 major ab T cell subsets. CD8$^+$ cytotoxic T cells show differential usage compared to the other T cell subset but are also substantiated by fewer cells. (C) Junctional length of TRA rearrangements of the 4 major ab T cell subsets. Junctional regions with dominant TRAV genes in CD8$^+$ cytotoxic T cells are 13 and 14 amino acids long. (D) TRG transcripts in CD8$^+$ cytotoxic T cells have a skewed junctional length with 16 amino acid length (top) and a conserved motif (bottom) (E) The majority of TRG rearrangements in CD8$^+$ cytotoxic T cells involved cassette 2 (TRGV2-2/TRGJ2-2). Genes are displayed in order of genomic location and colored by cassette.

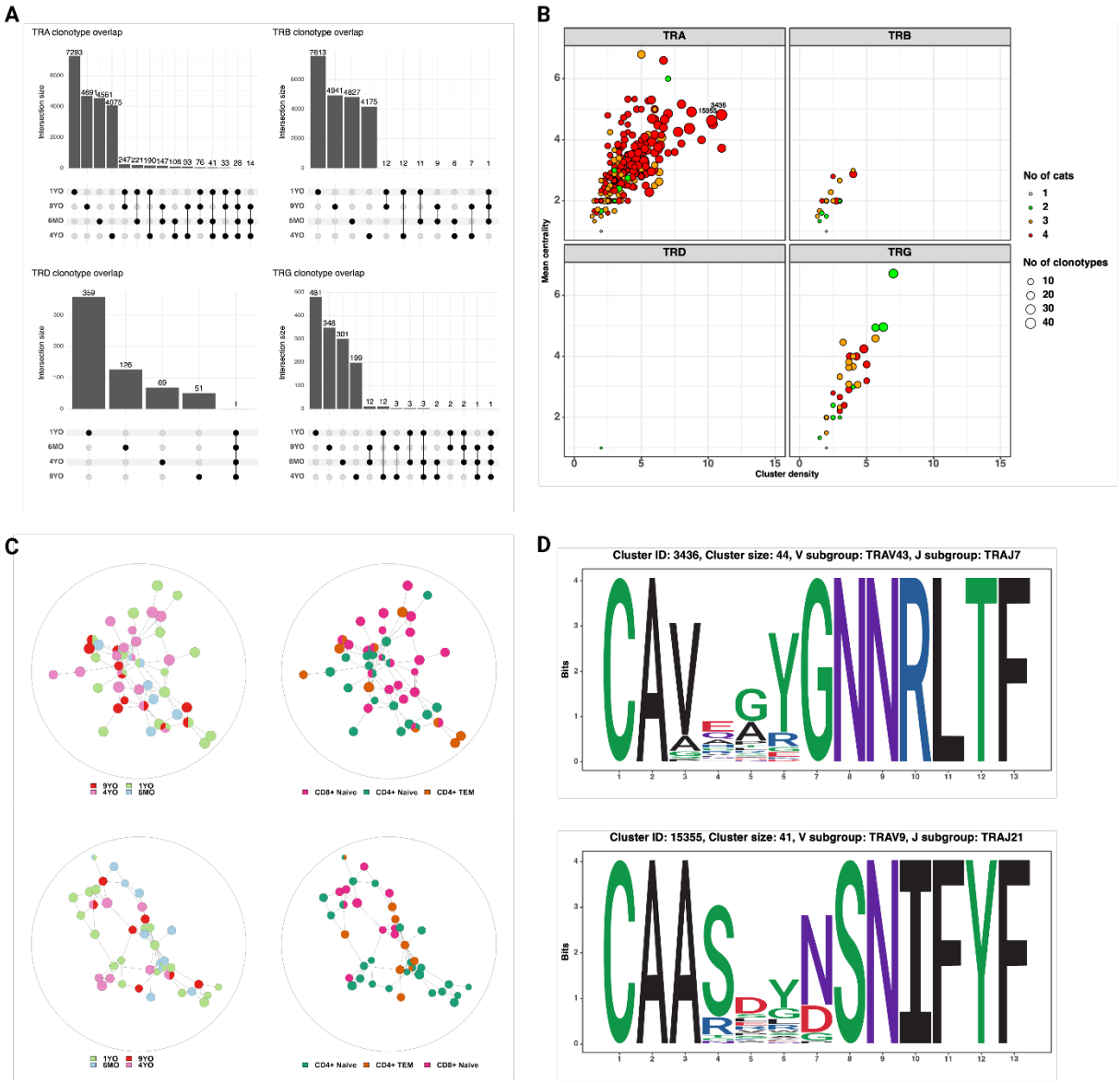

Figure 6. (A) Shared clonotypes across 4 cats. (B) Characterization of clusters based on mean centrality and cluster density. (C) Representative examples of TRA clusters with high centrality and density.

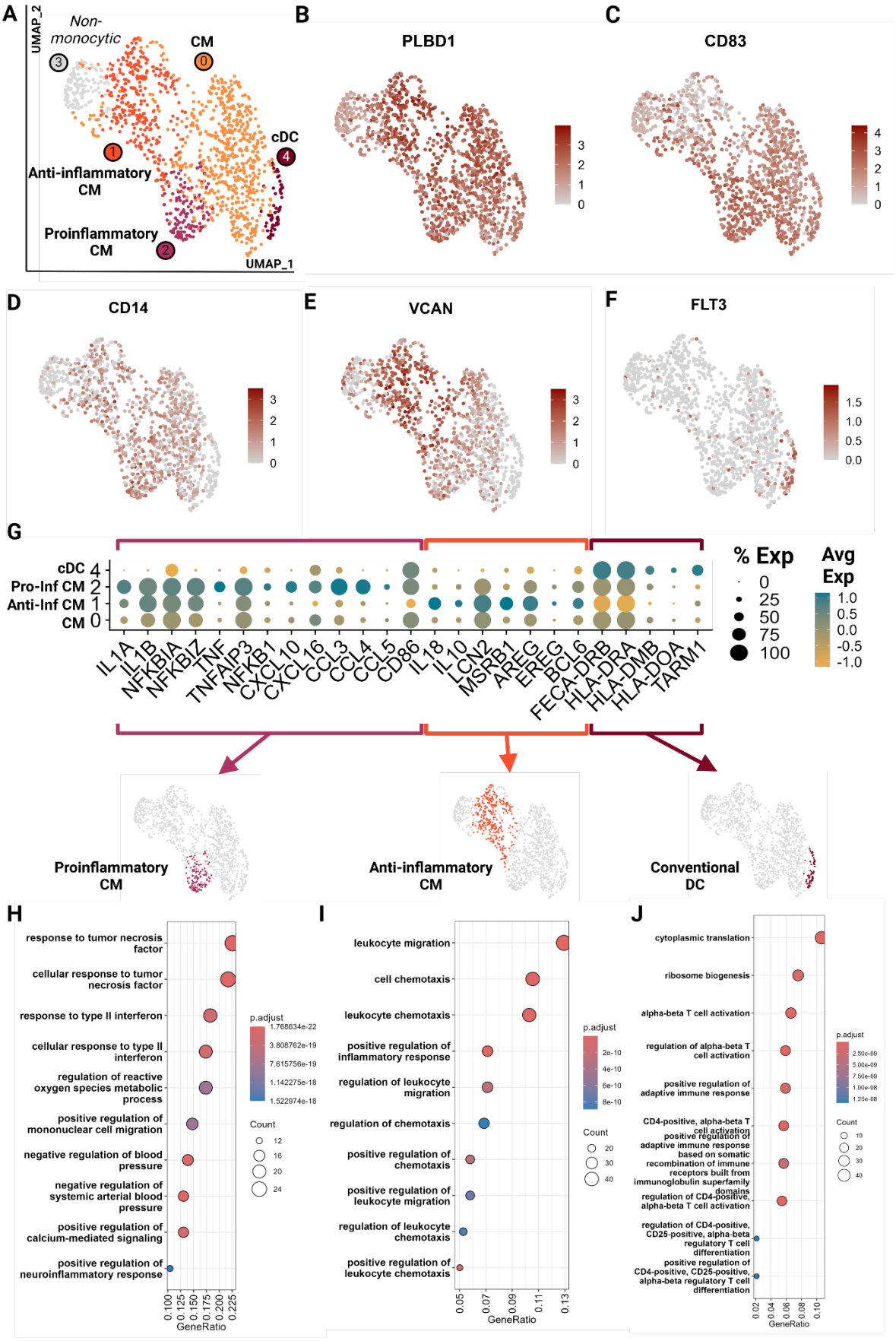
A
UMAP_2
Non-monocytic
CM
cDC
Anti-inflammatory CM
Proinflammatory CM
UMAP_1
B
PLBD1
C
CD83
D
CD14
E
VCAN
F
FLT3
G
cDC
Pro-Inf CM
Anti-Inf CM
CM
IL1A
IL1B
NFKBIA
NFKBIZ
TNF
TNFAIP3
NFKB1
CXCL10
CXCL16
CCL3
CCL4
CCL5
CD86
IL18
IL10
LCN2
MSRB1
AREG
EREG
BCL6
FECA-DRB
HLA-DRA
HLA-DMB
HLA-DOA
TARM1
% Exp
Avg Exp
Proinflammatory CM
Anti-inflammatory CM
Conventional DC
H
response to tumor necrosis factor
cellular response to tumor necrosis factor
response to type II interferon
cellular response to type II interferon
regulation of reactive oxygen species metabolic process
positive regulation of mononuclear cell migration
negative regulation of blood pressure
negative regulation of systemic arterial blood pressure
positive regulation of calcium-mediated signaling
positive regulation of neuroinflammatory response
GeneRatio
p.adjust
Count
I
leukocyte migration
cell chemotaxis
leukocyte chemotaxis
positive regulation of inflammatory response
regulation of leukocyte migration
regulation of chemotaxis
positive regulation of chemotaxis
positive regulation of leukocyte migration
regulation of leukocyte chemotaxis
positive regulation of leukocyte chemotaxis
GeneRatio
p.adjust
Count
J
cytoplasmic translation
ribosome biogenesis
alpha-beta T cell activation
regulation of alpha-beta T cell activation
positive regulation of adaptive immune response
CD4-positive, alpha-beta T cell activation
positive regulation of adaptive immune response based on somatic recombination of immune receptors built from immunoglobulin superfamily domains
regulation of CD4-positive, alpha-beta T cell activation
regulation of CD4-positive, CD25-positive, alpha-beta regulatory T cell differentiation
positive regulation of CD4-positive, CD25-positive, alpha-beta regulatory T cell differentiation
GeneRatio
p.adjust
Count

878 **Figure 7.** Feline circulating monocytes include classical monocytes with more differentiated
879 clusters with traditional proinflammatory and unconventional anti-inflammatory phenotypes.
880 Unsupervised clustering revealed 5 clusters. (A) UMAP of scRNA-seq atlas of monocytes. (B-
881 F) UMAP of monocytes colored by expression levels of canonical markers. (G) Dot plot of
882 genes of monocytic phenotypes across the 4 monocytic clusters. (H-J) Dot plots of top GO
883 biological process terms called based on sets of positive differentially expressed genes
884 identified via Seurat *FindMarker* function (Wilcoxon rank sum, *Adj P <0.05*). Classical
885 monocyte, CM; Conventional dendritic cell, cDC; Pro-inf, proinflammatory; Anti-inf, anti-
886 inflammatory.

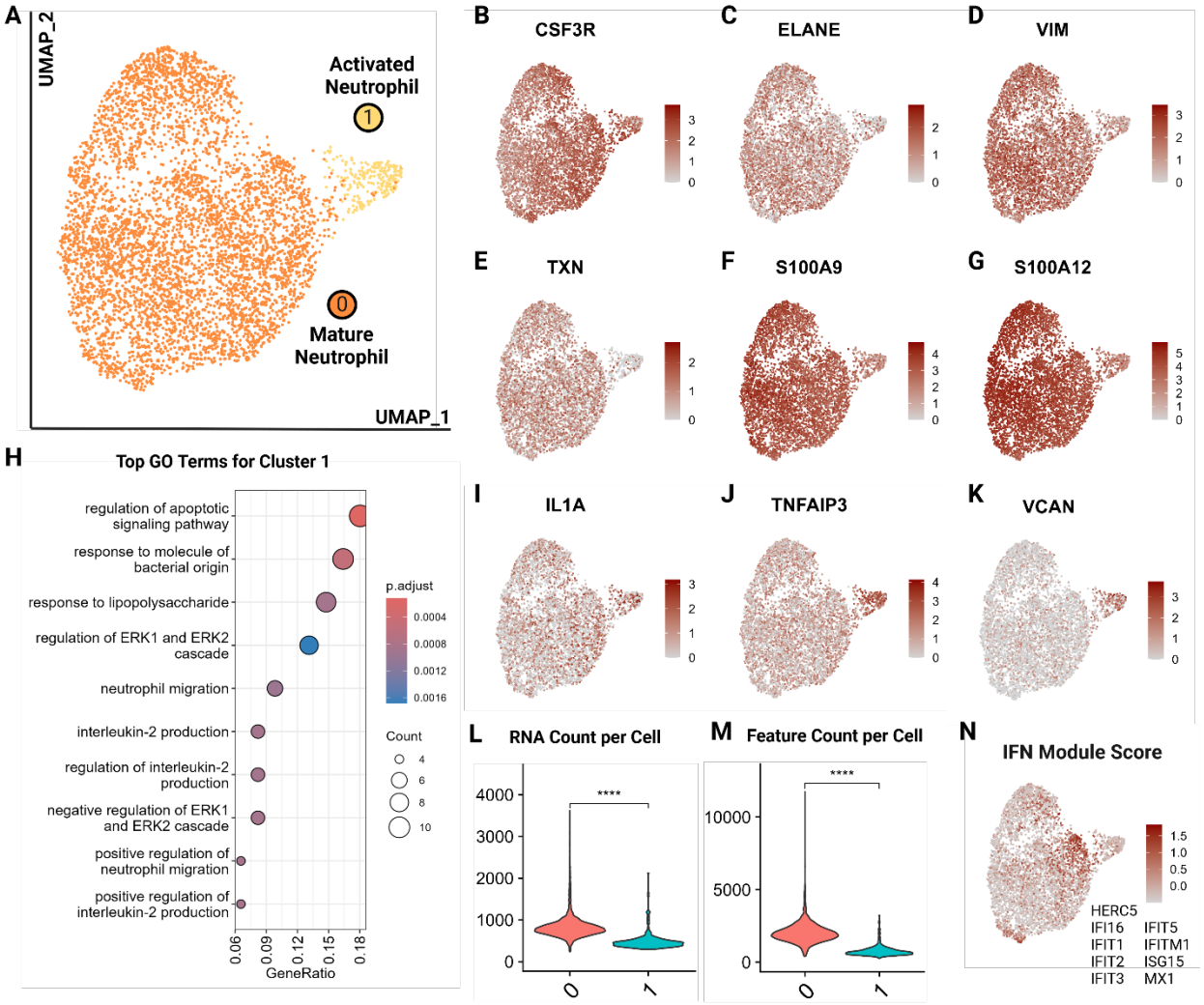

Figure 8. Feline circulating neutrophils separate into 2 clusters based on activation state. (A) UMAP of scRNA-seq atlas of neutrophils. (B-G) UMAP of neutrophils colored by expression levels of canonical and functional neutrophil markers. (H) Dot plots of top GO biological process terms in cluster 1 called based on sets of positive differentially expressed genes identified via Seurat *FindMarker* function (Wilcoxon rank sum, Adj $P < 0.05$). (I-K) UMAP of neutrophils colored by expression levels of select differentially upregulated genes in cluster 1. (L,M) Violin plots of RNA counts and feature (unique RNA) counts per cell by cluster; (****) indicates P value less than 0.001 by T-test. (N) UMAP of neutrophils colored by interferon (IFN) gene composite score per cell; genes included are named in figure.